# Convectively Coupled Kelvin Waves and Tropical Cyclogenesis: Connections through Convection and Moisture

QUINTON A. LAWTON<sup>®</sup> AND SHARANYA J. MAJUMDAR<sup>a</sup>

<sup>a</sup> Rosenstiel School of Marine, Atmospheric and Earth Science, University of Miami, Miami, Florida

(Manuscript received 7 January 2023, in final form 11 March 2023, accepted 20 March 2023)

ABSTRACT: Recent research has demonstrated a relationship between convectively coupled Kelvin waves (CCKWs) and tropical cyclogenesis, likely due to the influence of CCKWs on the large-scale environment. However, it remains unclear which environmental factors are most important and how they connect to TC genesis processes. Using a 39-yr database of African easterly waves (AEWs) to create composites of reanalysis and satellite data, it is shown that genesis may be facilitated by CCKW-driven modifications to convection and moisture. First, stand-alone composites of genesis demonstrate the significant role of environmental preconditioning and convective aggregation. A moist static energy variance budget indicates that convective aggregation during genesis is dominated by feedbacks between convection and longwave radiation. These processes begin over two days prior to genesis, supporting previous observational work. Shifting attention to CCKWs, up to 76% of developing AEWs encounter at least one CCKW in their lifetime. An increase in genesis events following convectively active CCKW phases is found, corroborating earlier studies. A decrease in genesis events following convectively suppressed phases is also identified. Using CCKW-centered composites, we show that the convectively active CCKW phases enhance convection and moisture content in the vicinity of AEWs prior to genesis. Furthermore, enhanced convective activity is the main discriminator between AEW-CCKW interactions that result in genesis versus those that do not. This analysis suggests that CCKWs may influence genesis through environmental preconditioning and radiative-convective feedbacks, among other factors. A secondary finding is that AEW attributes as far east as central Africa may be predictive of downstream genesis.

SIGNIFICANCE STATEMENT: The purpose of this work is to investigate how one type of atmospheric wave, known as convectively coupled Kelvin waves (CCKWs), impacts the formation ("genesis") of tropical cyclones. Forecasting of genesis remains a significant challenge, so identifying how CCKWs influence this process could help improve forecasts and give communities greater lead times. Our results show that CCKWs could temporarily make genesis more likely by increasing atmospheric moisture content and convective activity. While not all CCKWs lead to genesis, those that do are associated with a particularly strong increase in convection. This provides a potential tool for forecasters monitoring CCKWs and TC genesis in real time and motivates follow-up work on this topic in numerical models.

KEYWORDS: Atlantic Ocean; Convection; Kelvin waves; Atmospheric waves; Tropical cyclones; Reanalysis data

### 1. Introduction

The formation of tropical cyclones (TCs), known as tropical cyclogenesis or "genesis," has been a topic of inquiry for several decades and remains a substantial forecasting challenge (e.g., Cangialosi et al. 2020; Cangialosi 2022). Recent work has sought to quantify the role of intraseasonal oscillations and equatorial waves on genesis as one way of improving midrange forecasts. One promising avenue has been research into convectively coupled Kelvin waves (CCKWs), which have been shown to have a pronounced influence on African easterly waves (AEWs) and TC genesis itself (Ventrice et al. 2012a,b; Ventrice and Thorncroft 2013; Schreck 2015, 2016; Mantripragada et al. 2021; Lawton et al. 2022). Despite this, the mechanisms connecting CCKWs and genesis processes are still poorly understood. This study will address this knowledge gap by focusing on the potential connections between these phenomena through atmospheric convection and moisture.

Corresponding author: Quinton A. Lawton, quinton.lawton@earth.miami.edu

AEWs and CCKWs have fundamental ties to convection. AEWs are synoptic-scale systems that move westward over tropical Africa and the Atlantic Ocean (Burpee 1972; Reed et al. 1977; Kiladis et al. 2006), serving as the source for over 60% of TCs in the Atlantic basin (Russell et al. 2017). There is now sizeable evidence that moist convection is essential for both the growth and propagation of AEW vortices (Hall et al. 2006; Berry and Thorncroft 2012; Russell and Aiyyer 2020; Russell et al. 2020). The presence of moist convection within the AEW trough can also modify wave characteristics that make genesis more or less likely; this includes the wave's midlevel circulation, its spatial and vertical moisture distributions, and its favorability to sustained mesoscale convective systems (MCSs) and other convective activity (Wang et al. 2010; Hopsch et al. 2010; Berry and Thorncroft 2012; Peng et al. 2012; Leppert et al. 2013a,b; Brammer and Thorncroft 2015; Brammer et al. 2018; Núñez Ocasio et al. 2020, 2021). Meanwhile, CCKWs are equatorial waves that propagate eastward and whose vertical motions are directly coupled to convective activity (Gruber 1974; Takayabu 1994; Wheeler and Kiladis 1999; Kiladis et al. 2009). These waves consist of a convectively enhanced ("active") phase and a convectively suppressed

DOI: 10.1175/MWR-D-23-0005.1

("suppressed") phase. In the troposphere, each phase is collocated with humidity and vertical motion anomalies that have a pronounced westward tilt with height (Straub and Kiladis 2002; Yang et al. 2007; Kiladis et al. 2009). CCKWs that propagate into the Atlantic typically originate from either the Pacific or South America (Mayta et al. 2021); these waves can modulate precipitation in these areas (Mounier et al. 2007; Mekonnen et al. 2008) and are hypothesized to influence AEW activity and barotropic growth processes (Ventrice and Thorncroft 2013; Sridhar Mantripragada et al. 2021; Lawton et al. 2022).

Research over the last decade has established a statistical relationship between CCKWs and TC genesis, with genesis favored in a 1-3-day window following a CCKW's active phase (Ventrice et al. 2012a; Schreck 2015). Several theories have been put forth to explain this relationship and the pronounced lag time. Ventrice et al. (2012b) studied the impacts of CCKWs on the Atlantic environment and argued that an increase in low-level potential vorticity, total column water vapor (TCWV), and modifications to vertical wind shear all could impact the favorability of genesis. For example, CCKW-associated easterlies can add to the climatological easterly shear in the east Atlantic and can partially oppose climatological westerly wind shear in the west Atlantic. Schreck (2016) used a semi-Lagrangian framework to show that the westward tilt of a CCKW's zonal wind anomalies may cause relative vorticity around incipient disturbances to "build up" from the lower troposphere to the upper troposphere. They argued that this buildup, in addition to an enhancement of anticyclonic outflow aloft, could explain the CCKW-TC relationship and the observed 1–2-day lag. More recently, Lawton et al. (2022, hereafter L22) used an AEW-following framework to study the impact of CCKWs on AEWs that do not develop into TCs (nondevelopers). In addition to confirming the relative vorticity buildup shown by Schreck (2016), they found that CCKWs temporarily increased the convective coverage and midtropospheric humidity surrounding the AEW trough. L22 suggested that CCKW-related modifications to specific humidity and convection may play a more direct role in promoting genesis than previously realized.

Despite these hypotheses, a clear connection between CCKWs, their environmental influences, and genesis processes has yet to be established. It is also unclear why some CCKW-AEW interactions result in genesis while others do not. In this paper, we hypothesize that one potential pathway connecting these phenomena is through the modulation of convection and moisture by CCKWs (e.g., Ventrice et al. 2012a; L22). This is in part due to substantial evidence that convection and moisture play a critical role in genesis. Several numerical modeling studies have suggested that environmental premoistening to near saturation is necessary to maintain sustained deep convection, which promotes the low-level vortex spin up of TCs (Nolan 2007; Wang 2012, 2014). This has been corroborated by observational data showing a gradual increase in the lower- and middle-tropospheric moisture (Komaromi 2013; Zawislak and Zipser 2014) and an increase in the coverage of convection and precipitation (Leppert et al. 2013a,b; Zawislak 2020) in the days prior to genesis. Furthermore, idealized and case modeling studies have emphasized

the importance of cloud–radiative feedbacks to convective aggregation (clustering), including during genesis (e.g., Davis 2015; Wing et al. 2016; Carstens and Wing 2020; Ruppert et al. 2020; Yang and Tan 2020; Yang et al. 2021; Zhang et al. 2021; Wu et al. 2021; Wing 2022). Cloud–radiative feedbacks and convective aggregation enhance spatial gradients of heating, driving a thermally direct transverse circulation that imports angular momentum and moisture toward the incipient TC center (Wang 2018; Ruppert et al. 2020). Given the apparent importance of these processes to genesis, it is likely that any external factor that modifies the distribution of convection or moisture around an initial disturbance could subsequently impact genesis. This motivates our exploration of the CCKW and TC genesis relationship through convection and moisture.

Here we investigate the relationship between CCKWs and TC genesis in reanalysis and satellite data, using a 39-yr database of AEW and CCKW passages. Our primary goal is to ascertain how CCKWs modify environmental characteristics around AEWs prior to genesis, and to determine possible connections between these changes and genesis processes. A secondary goal is to quantify the depiction of genesis and associated AEW characteristics. To contextualize the influence of CCKWs, we will first study the characteristics that make AEWs favorable to genesis (section 3) and the genesis process itself (section 4), prior to focusing on CCKWs (section 5).

#### 2. Data and methods

### a. Data and AEW-CCKW identification

The fifth-generation ECMWF Reanalysis (ERA5; Hersbach et al. 2020) dataset is used for most environmental fields in this study. Following L22, the fields are obtained at a 6-hourly resolution, on a  $1^{\circ} \times 1^{\circ}$  grid, with 19 pressure levels. These fields are typically represented as climatological anomalies (as in L22). The fields used to compute moist static energy (MSE) and its related budget terms are saved at a higher resolution  $(0.25^{\circ} \times 0.25^{\circ}$  grid, 36 pressure levels). NOAA GridSat-B1 data (Knapp et al. 2011;  $0.25^{\circ} \times 0.25^{\circ}$  grid) is used for convective coverage calculations and CCKW identification. Convective coverage is defined as the fraction of grid boxes within a given radius of the AEW that have brightness temperature values of 240 K<sup>1</sup> or lower (as done by Leppert et al. 2013a,b; L22).

We use the same AEW tracks and CCKW passage information from the dataset published by L22. This climatology is over the months July–September from 1981 to 2019. AEWs are tracked using a modified curvature vorticity term at 700 hPa, averaged within 600 km of each reanalysis grid point. AEWs are classified as "developers" if they have a center located within 500 km of a TC genesis point in the HURDAT database (Landsea and Franklin 2013). AEWs associated with genesis events west of 60°W are not included in this analysis.

Active and suppressed CCKW phases are identified relative to the AEW tracks. First, we conduct Kelvin filtering of Grid-Sat-B1 brightness temperature  $(T_b)$  using the method of

<sup>&</sup>lt;sup>1</sup> Other brightness temperature thresholds—from 210 through 250 K—were also tested and had no impact on our results.

Wheeler and Kiladis (1999). We choose observational  $T_b$  to avoid reanalysis-dependent limitations in CCKW representation (e.g., Chien and Kim 2023) and because we are most interested in Kelvin waves that are convectively coupled. The Kelvin band is bounded by zonal wavenumbers of 1–14, a temporal period of 2.5–20 days, and an equivalent depth of 8–90 m. Then, the 0°–10°N average of Kelvin-filtered  $T_b$  is computed at the longitude of each AEW point. Maxima and minima of this time series are identified as CCKW phases if they exceed  $\pm 1$  standard deviation of the climatological value. More details on the AEW and CCKW identification methods can be found in L22.

Composites shown throughout this analysis are constructed relative to a "day 0" reference point. Day 0 can either be the time at which the center of the tracked AEW is aligned in longitude with that of a CCKW's active/suppressed phase ("CCKW-relative"), or the time of genesis as defined by the HURDAT database ("genesis-relative"). However, AEW characteristics change dramatically as they exit the coast of Africa. As a result, composites are adjusted to the longitudinal climatology of AEWs as done by L22. The subtracted AEW climatology differs depending on the category of AEW being analyzed. Genesis-relative composites are adjusted to the climatology of developing AEWs only, and composites of nondeveloping AEWs are adjusted by the nondeveloping climatology. When comparisons between developers and nondevelopers are made (section 5c), we adjust both sets of samples identically, using a combined climatology of favorable developing and nondeveloping AEWs. Ultimately, the selected climatological adjustment has only a minor impact on our results.

### b. Logistic regression model

As has been noted in previous AEW climatologies (e.g., Hopsch et al. 2010; Agudelo et al. 2011; Brammer and Thorncroft 2015), the vast majority of AEWs are relatively weak systems that are not associated with genesis. This presents an inherent problem when attempting to compare nondeveloping and developing AEWs as they pass CCKWs. Thus, it is advantageous to focus on AEWs that are "favorable" to genesis. To do so, we follow Brammer and Thorncroft (2015) in using logistic regression. This is a classification technique where a predictive model is trained on input data to predict a binary outcome: in this case, TC genesis. Once trained, the predictive model assigns each AEW a probability p of undergoing genesis that ranges from 0 to 1: we refer to this as the "favorability score." A value of p = 0.5 is chosen as the cutoff between "unfavorable" and "favorable" AEWs.

Inputs are selected from a range of climatological and environmental fields surrounding the AEW, with environmental fields averaged within 500 km of the AEW.<sup>2</sup> In total, 10 different logistic regression models are built, each using a different input longitude (spaced every 10°, from 40°W to 30°E). For

the logistic regressions run over land and at 20°W, only genesis events east of 40°W are considered. For those run over the ocean, only genesis events within 20° of the input longitude are considered. More background on our application of logistic regression can be found in the appendix.

### c. MSE variance budget and application

To quantify convective–radiative feedbacks, we use a budget analysis of the *spatial variance* of column-integrated *frozen* moist static energy (henceforth, MSE). This budget was first developed by Wing and Emanuel (2014) to quantify sources of convective self-aggregation, a potential precursor to genesis. Such a budget has been used to study genesis in idealized models (Carstens and Wing 2020; Wing 2022), global simulations (Zhang et al. 2021), and convection-resolving models (Ruppert et al. 2020; Wu et al. 2021). It has also been used for TC intensification in climate simulations (Wing et al. 2019) and in reanalysis data (Dirkes et al. 2023). The consolidation of convection and moisture during self-aggregation results in an increase in the spatial variance of MSE.

The column-integrated MSE is given by

$$\hat{h} = \frac{1}{g} \int_{\text{lhPa}}^{920\text{hPa}} (c_p T + gz + L_v r_v - L_f r_i) dp, \tag{1}$$

where  $\hat{h}$  is the column-integrated MSE, g is gravity (9.81 m s<sup>-1</sup>),  $c_p$  is the specific heat of dry air (1005.7 J kg<sup>-1</sup> K<sup>-1</sup>),  $L_v$  is the enthalpy of vaporization (2.5 × 10<sup>6</sup> J kg<sup>-1</sup>),  $L_f$  is the enthalpy of fusion (3.3 × 10<sup>5</sup> J kg<sup>-1</sup>), and T, z,  $r_v$ , and  $r_i$  are temperature, geopotential height, water vapor mixing ratio, and mixing ratio of all ice phase condensates, respectively. We retain the 920-hPa integration boundary from Wing et al. (2019), as some of our budgets are computed over African terrain where sub-1000-hPa pressure levels often intersect with the surface.

Next,  $10^{\circ} \times 10^{\circ}$  boxes<sup>3</sup> are constructed around each tracked AEW center, encompassing 1600 grid points. The budget of  $\hat{h}$  variance is approximated<sup>4</sup> within this box using

$$\frac{1}{2}\frac{\partial \hat{h}'^2}{\partial t} \cong \hat{h}' F_k' + \hat{h}' N_L' + \hat{h}' N_S' - \hat{h}' (\widehat{u \cdot \nabla h}), \tag{2}$$

where  $\hat{h}'$  is the MSE anomaly within the  $10^{\circ} \times 10^{\circ}$  box,  $F_{k}'$  is the anomaly of net surface enthalpy flux, and  $N_{L}'$  and  $N_{S}'$  are the anomalies of net column longwave and shortwave radiation flux convergence, respectively. The left-hand term represents the tendency of the box variance of MSE. On the right, the first term represents surface flux feedbacks, the second and third terms represent radiative feedbacks, and the last term is a compensating advective term. The advective term must be computed as a residual due to the challenges of computing advection from offline reanalysis output; as a result, this term may include other sources

<sup>&</sup>lt;sup>2</sup> The radius of 500 km was chosen to correspond to the work of Brammer and Thorncroft (2015) and differs slightly from the 600-km radii used for compositing elsewhere in this paper. However, sensitivity testing using varying radii, including 600 km, revealed that this selection has little impact on our final conclusions.

<sup>&</sup>lt;sup>3</sup> This was chosen to make the MSE budget results more comparable to previous work. Such a box size is similar to, though slightly smaller than, the 600-km averaging radii used for environmental variables.

<sup>&</sup>lt;sup>4</sup> This an approximation because this budget neglects a kinetic energy generation term (Wing et al. 2019).

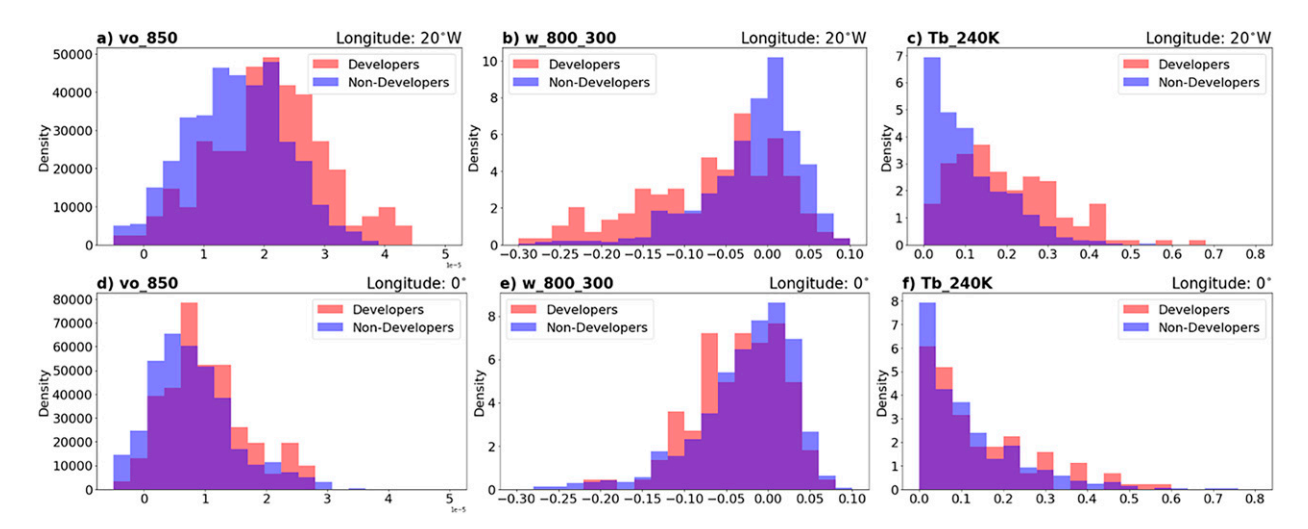


FIG. 1. Probability density functions (PDFs) of select variables averaged within 500 km of a tracked AEW center, comparing developing AEWs (red) to that of nondeveloping AEWs (blue). Overlapping bins are colored purple. The first row is for variables at 20°W: (a) relative vorticity at 850 hPa, (b) vertical motion (Pa s<sup>-1</sup>) averaged between 800 and 300 hPa, and (c) the percent coverage of convection using 240 K as a threshold. (d)–(f) As in (a)–(c), but at 0°W.

of error. Conceptually, this budget illustrates that the spatial variance of MSE increases when anomalies in MSE are correlated with MSE generation terms.

### d. Statistical methods

Bootstrapping methods are used to evaluate statistical significance. For genesis-relative composites of environmental fields, we evaluate null hypothesis 1: that observed changes in these composites are no different than what would occur if a random point in time was used for day 0. To test this, we build 1000 composites using a random time for day 0 in place of the time of genesis. A result is determined to be statistically significant if the original composite is above or below 975 of the random composites. For other composites, we evaluate null hypothesis 2: that the samples in group 1 are indistinguishable from those in group 2. A result is considered statistically significant at a given lag time and level if the 975 of the bootstrapped composites for group 1 are above or below 975 of those of group 2.

A slightly different statistical significance method is used to evaluate the CCKW-TC lags presented in section 4. Here, the null hypothesis is that the number of TCs contained in each CCKW-lag bin are no different than that expected to occur in each via random chance. This is tested by building 10 000 new CCKW-TC lag distributions, each using random time values for the active/suppressed CCKW phases. The 95% climatological confidence interval is bounded by the 275th highest and lowest TC counts for each bin. Note that some "jumps" are evident in these bounds due to the whole number nature of TC counts.

# 3. Quantifying the favorability of an AEW to undergo TC genesis

In this section, we use logistic regressions to quantify the favorability of AEWs to undergo TC genesis. There are two primary goals of this analysis. First and foremost, it is used to isolate favorable waves so that more robust comparisons of AEW-CCKW interactions can be made in section 5. Second, it can provide insight into the characteristics of AEWs associated with genesis. While this has been evaluated extensively for AEWs over the Atlantic and western Africa (i.e., Hopsch et al. 2010; Berry and Thorncroft 2012; Brammer and Thorncroft 2015), it is much less studied for AEWs over central and eastern Africa.

The signs and values of model output coefficients align with what is already known about AEW favorability to genesis (see the appendix and Table A1). This is further evidenced by the distributions of select environmental variables for developing and nondeveloping AEWs at 20°W (Figs. 1a–c). In general, the distributions of low-level vorticity, convection, and upward vertical motion at 20°W are shifted to higher magnitudes for developing AEWs. They also appear to have more variability than their nondeveloping counterparts.

Similar trends hold for logistic regression models run using other input longitudes: AEWs that are stronger, moister, and more convectively active tend to be more likely to undergo genesis. However, differences between AEW characteristics are more subtle over the African continent than over the ocean. For example, the distributions of convection and vertical motion for AEWs over central Africa (0°, Figs. 1d–f) are very similar for developing and nondeveloping AEWs. Nevertheless, values for developing AEWs are still shifted toward higher magnitudes at 0°, especially for the 850-hPa vorticity averages (Fig. 1d).

One way to quantify model skill is through its receiver operator characteristic (ROC) curve, which shows the rate the model defines true positives relative to false positives (Fig. 2a). The skill of a completely random guess is represented by a y = x line. The greater the model skill, the greater the area under the curve (AUC) is. As shown in Fig. 2, model skill is clearly dependent on input longitude. Regressions run for AEWs over the

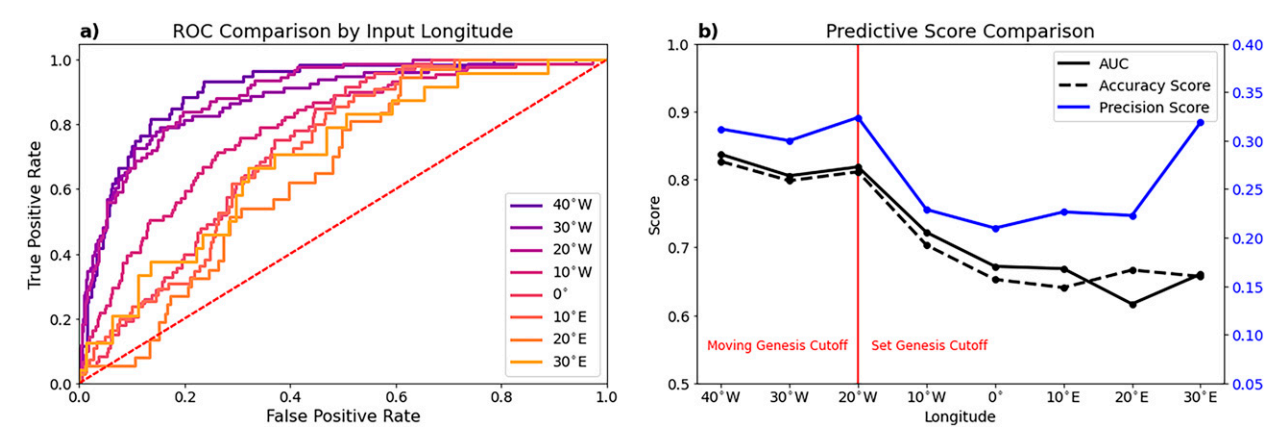


FIG. 2. Summary of the measured predictive skill of the logistic regression models. (a) Comparison of the receiver operator characteristic (ROC) curves for different input longitudes, showing the ratio of true to false positives. The red dashed line indicates the predictive skill of a random guess. (b) Comparison of various metrics of model predictive skill. This includes the area under the ROC curve (AUC; black solid line), an accuracy score (black dashed line), and a precision score (blue solid line). While genesis must occur by 40°W to count for the binary classification for model runs over land, points over the ocean have a moving cutoff that is 20°W to the west of the input longitude.

coastline and ocean have significantly larger AUCs than those run over land (Fig. 2b), and thus greater skill. A similar trend can also be seen in the accuracy and precision scores (Fig. 2b). The accuracy score indicates the fraction of correct predictions, whereas the precision score measures the skill of the model in *avoiding false positives* (i.e., predicting TC genesis when it does not occur). One reason for this trend could simply be that AEWs are inherently farther away from genesis when they are over land than over the ocean. Recall that the ocean-based regressions (20°W and west) have a moving genesis threshold such that genesis must occur within 20° longitude of the input point. Perhaps relatedly, the skill is quite similar between the ocean-based regressions.<sup>5</sup>

Nevertheless, these regressions show remarkable skill in predicting outcomes of genesis, even over central Africa. The AUC for ocean-based regressions ( $\sim$ 0.8–0.83) is comparable, if slightly lower, than what Brammer and Thorncroft (2015) found for their regression model at 20°W (Fig. 2b; cf. their Fig. 5). But even the regressions run at 0° and 10°E show skill, with AUCs just below 0.70 and an ROC curve showing noteworthy skill over a random guess. Another way to visualize this is via the normalized distributions of AEW favorability scores for developing and nondeveloping AEWs (Fig. 3). For the 40°-10°W regressions (Figs. 3a-d), there is a distinct separation between the distributions, with most developing waves having favorability scores above the 0.5 classification threshold and vice versa for nondeveloping AEWs. A demarcation is also visible in the 0° and 10°E regressions (Figs. 3e,f), with slightly more overlap, suggesting these still have some skill.

The regressions run at longitudes farther east (Figs. 3g,h) exhibit little to no skill.

Comparing favorable AEWs themselves provides additional evidence that an AEW's characteristics over central and western Africa can be predictive of genesis. We construct comparisons of area-averaged environmental fields for favorable developing (Fig. 4) and nondeveloping AEWs (not shown). Composites using the 20°W regression classifications indicates that even over West Africa (20°W-0°), favorable AEWs have statistically significantly stronger low-level vorticity and a more convection-like divergence profile than nondeveloping AEWs (Figs. 4a-c). When we define favorable AEWs using the 0° regression, the differences in divergence, midlevel vorticity, and upper-level specific humidity extend into central Africa (Figs. 4d-f). Similar composites of vertical motion (not shown) suggest that this behavior is associated with AEWs that are more convectively active, which promotes a moister wave trough and could help support AEW growth (e.g., Russell et al. 2020; Russell and Aiyyer 2020).

Taken together, results from these logistic regressions indicate that the characteristics of AEWs *prior* to their exit from the coast of Africa are predictive of genesis well downstream. This demonstrates that a skillful logistic regression can be used to reduce the number of unimportant, weak AEWs for the analysis in section 5. These waves are important to eliminate when trying to isolate the impact of CCKWs on the AEW pathway to genesis. Due to the high skill seen for the 20°W regression and the use of a similar one in Brammer and Thorncroft (2015), it will be used to define the favorable waves for the analysis of AEW–CCKW interactions.

### 4. Process-oriented diagnostics of TC genesis in reanalysis data

We now proceed to an analysis of the AEW pathway to TC genesis. This is necessary to contextualize the impacts of CCKWs discussed later in section 5. We first use composites

<sup>&</sup>lt;sup>5</sup> An alternative set of logistic regressions were run where the ocean-based regressions required genesis to be at or east of 60°W, not the moving target presented here. In that case, the AUC and accuracy score increased steadily from east to west for the 10°–40°W regressions. This supports the hypothesis that predictive skill increases could be at least in part driven by the shorter time to genesis.

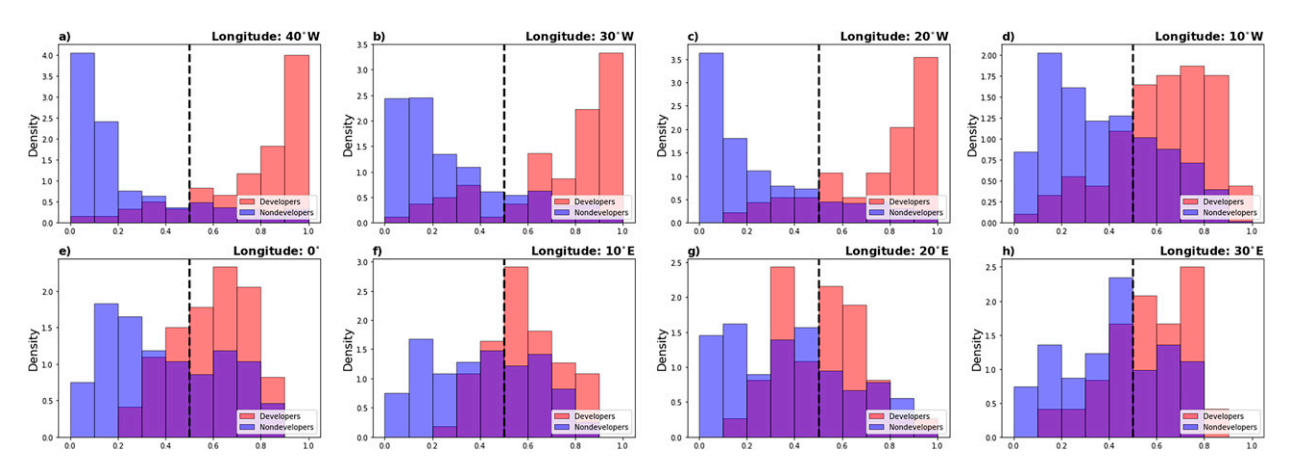


FIG. 3. Probability density functions (PDF) of genesis favorability scores, subset by whether genesis occurs (developers, red) or does not occur (nondevelopers, blue). Each graph represents the results of the logistic regression model run with input data at a distinct longitude: (a)–(d) longitudes  $40^{\circ}$ – $10^{\circ}$ W and (e)–(h) longitudes  $0^{\circ}$ – $30^{\circ}$ W. Scores are binned every 0.10, with the dashed black vertical line indicating the threshold for predicting genesis (i.e., genesis predicted if a score is at or greater than 0.5).

of all 153 genesis events in the AEW database to highlight that genesis is a multiday process. Following this, we leverage composites of MSE variance and its source terms to quantify their role in genesis.

Composites of ERA5 variables and convective coverage are oriented such that day 0 (right side) is the time of genesis (Fig. 5). Starting nearly two days prior to genesis, the average diabatic heating (thermodynamic residual "Q1"; Yanai et al. 1973) surrounding the AEW increases, the middle to upper troposphere warms, and the convective coverage increases significantly (Figs. 5a,c,e). Meanwhile, there is widespread moistening of the AEW trough at nearly all levels (Figs. 5b,f) and average relative vorticity from 1000 to 300 hPa increases in the 2 days preceding genesis (Fig. 5d). An anticyclonic

circulation also develops aloft  $\sim$ 1 day prior to genesis. Similar plots using other averaging radii (such as 600 km) were also created and show a similar progression to that of Fig. 5.

These results support the hypothesis of environmental preconditioning multiple days prior to genesis. The two day moistening trend seen in Figs. 5b and 5f is similar to what Zawislak and Zipser (2014) found in pregenesis systems using dropsonde data. It is also consistent with previous studies arguing that middle- and upper-level saturation helps accelerate the genesis process (Davis 2015; Nolan 2007). Furthermore, the observed increase in convective coverage (Fig. 5e) resembles a similar analysis in Leppert et al. (2013a,b), and is congruent with the increase in total precipitation area prior to genesis shown by Zawislak (2020). Notably, our composites

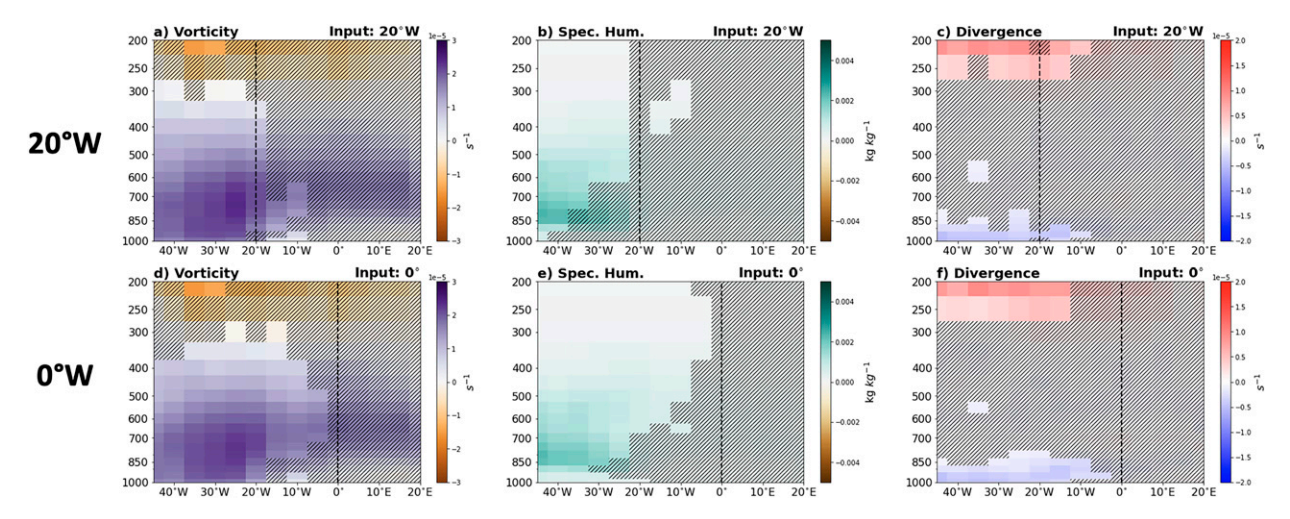


FIG. 4. The longitudinal evolution of variables averaged within 600 km of the tracked AEW center, composited every 5°, for favorable AEWs that result in genesis. AEW tracks are not dropped after genesis, and thus composites over the ocean may include AEWs for which genesis has already occurred. The first row depicts variables for favorable developing AEWs, with favorability defined using the logistic regression model at 20°W: (a) relative vorticity, (b) specific humidity, (c) divergence. (d)–(f) As in (a)–(c), but with favorability defined using the 0°W logistic regression model. Nonhatched regions are where these values are significantly different than those of favorable nondeveloping AEWs (95% threshold).

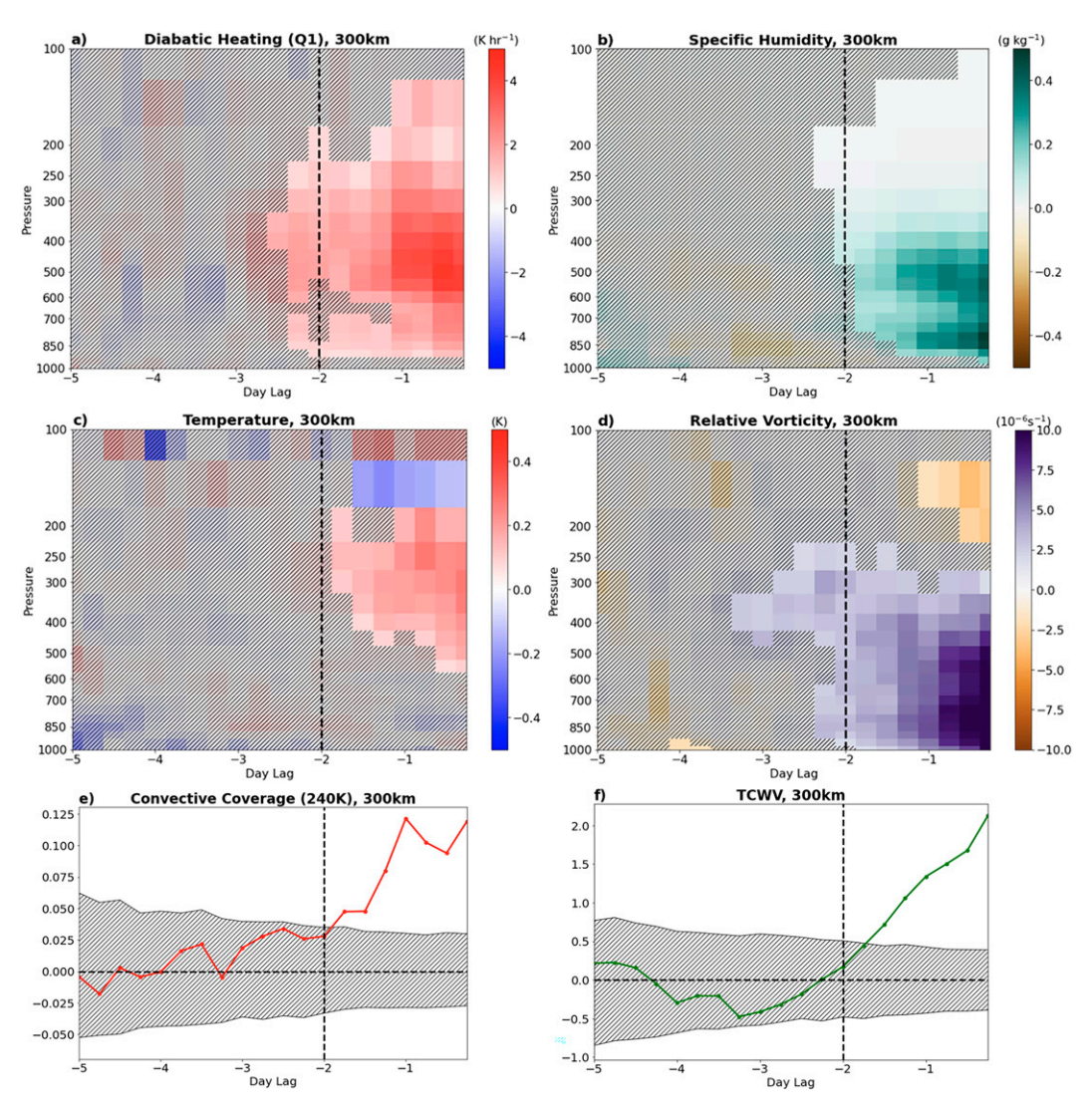


FIG. 5. Composites relative to genesis of (a) diabatic heating (Q1), (b) specific humidity, (c) temperature, (d) relative vorticity, (e) convective coverage, and (f) total column water vapor (TCWV) surrounding the AEW. Samples are averaged within 300 km of the tracked AEW centers. All genesis cases in the AEW database are included, with the longitudinal AEW climatology subtracted from each case. The *x* axis indicates the days out from genesis (day 0, right side). Nonsignificant areas at a 95% threshold, tested using null hypothesis 1, are hatched out.

indicate that diabatic heating is concentrated between 600 and 400 hPa (Fig. 5a). This corresponds to 4–7 km in altitude and is potentially associated with midlevel convection. Some studies have indicated that midlevel convection is an important driver of genesis, as it helps precondition the lower troposphere and spin up a low-level circulation (Fritz et al. 2016; Wang 2014). Additional evidence for this may be the two bands of specific humidity maxima seen in Fig. 5b, the upper one of which may be associated with midlevel convection. Finally, the development of a warm core in the upper troposphere, followed by the middle troposphere (Fig. 5c), agrees with observational data (Komaromi 2013; Zawislak and Zipser 2014).

We now turn to a MSE spatial variance budget to provide a clearer picture of convective-radiative feedbacks. Though the overall budget is computed over a  $10^{\circ} \times 10^{\circ}$  box surrounding AEWs, the terms in Fig. 6 are averaged over the innermost  $5^{\circ} \times 5^{\circ}$  box, as this encompasses most of the AEW's convective activity. The composites of MSE variance itself shows a pronounced increase in the two days leading up to genesis (Figs. 6a,b). The dominant source of the increase in MSE variance is the longwave radiative feedback term (Figs. 6c,d), which becomes elevated relative to climatology three days prior to genesis. While the surface flux feedback term has a smaller magnitude, it does increase substantially one day prior to genesis. Meanwhile, the shortwave radiation term does not play a significant role.

The spatial distributions of these terms are shown in Fig. 7. The MSE plots show the dramatic increase in MSE variance, with regions of elevated MSE (Figs. 7a,e) increasing

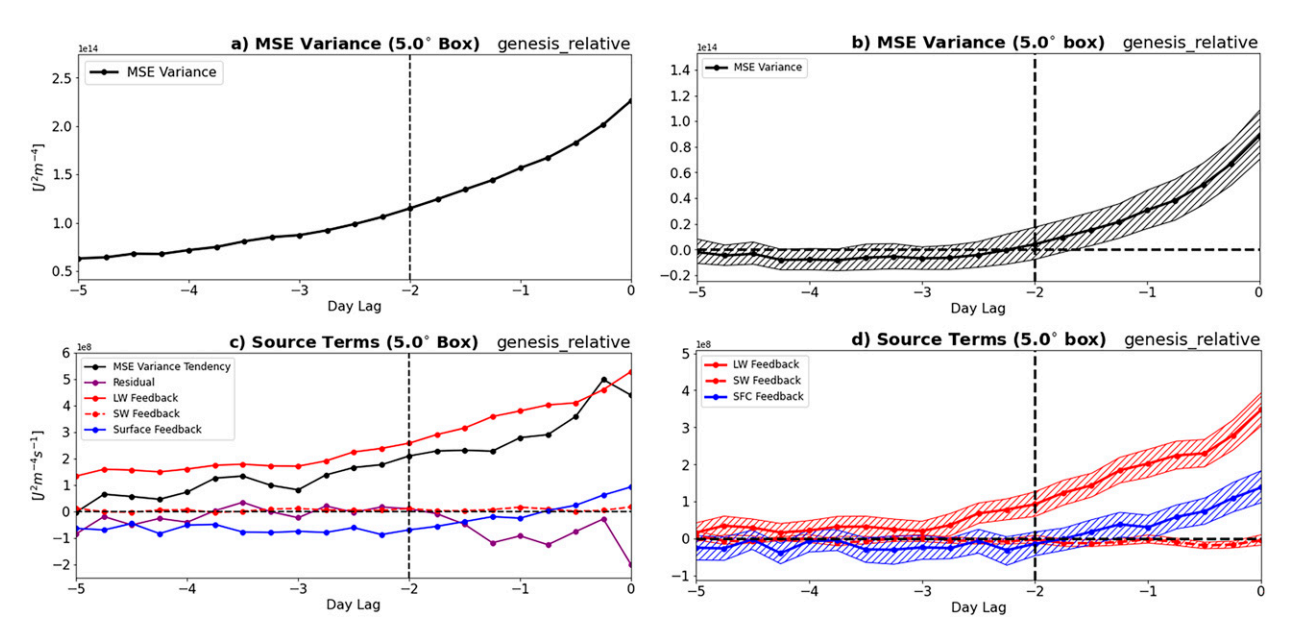


FIG. 6. Composites relative to genesis (day 0) of (a),(b) MSE variance and (c),(d) MSE variance budget terms. These terms are calculated using a  $5^{\circ} \times 5^{\circ}$  box surrounding the tracked AEW center. (left) Absolute values and (right) values adjusted for the AEW climatology. Bootstrapping is used to generate a 95% confidence interval for the climatology-adjusted plots and is shown as the hatched area in (b) and (d). The vertical dashed black line serves as a reference for 2 days prior to genesis.

in magnitude closer to genesis (Figs. 7i,m). Growth in longwave radiative feedbacks (Figs. 7c,g,k,o) is concentrated both near the center of the tracked AEW and at the periphery of the system, in particular the northwestern quadrant. An analysis of the underlying terms (not shown) shows that this is the result of net outward longwave radiation flux increasing in regions of high MSE (center) and decreasing in regions of low MSE (periphery). This promotes more convection where it already exists and suppresses it elsewhere. Furthermore, the surface feedback term, while negative in value at earlier times, increases significantly near the center of the AEW in the day prior to genesis (Figs. 7j,n). The positive values appear to wrap around the northwestern side of the system, associated with stronger surface winds (wind barbs). This suggests the importance of the longwave radiation feedback prior to the developing of a pronounced surface circulation.

These results provide further evidence of the importance of radiative–convective feedbacks to the genesis process. In the days preceding genesis, the largest source of MSE variance in our composites was longwave radiation feedbacks (Figs. 6 and 7). This is congruent with recent work by Dirkes et al. (2023) on intensifying TCs in reanalysis data, which showed that radiational feedbacks were more important than surface flux feedbacks in weak TCs. A radial gradient in diabatic heating, in this case reinforced by the reduction of longwave cooling by convective clouds near the center of the developing AEWs, can help drive a thermally direct transverse circulation (e.g., Wang 2018; Ruppert et al. 2020; Wu et al. 2021; Wing 2022). This promotes TC vortex spinup through the convergence of angular momentum and humidity toward the center. While smaller in magnitude, it does appear that the surface

feedback term becomes more important starting about one day prior to genesis.

To our knowledge, this is the first analysis of a MSE budget for TC genesis in reanalysis data. However, the use of reanalysis data comes with caveats. In particular, reanalysis has known errors in representing TCs (e.g., Schenkel et al. 2017; Bian et al. 2021; Jones et al. 2021), and results presented here may be influenced by specific characteristics of ERA5 reanalysis such as parameterization schemes and data assimilation. One potential impact is on the relative magnitudes of feedback terms. For example, Dirkes et al. (2023) studied MSE variance budgets for intensifying TCs and found there to be distinct differences in the magnitude of MSE and related feedback terms across several reanalysis datasets. They also argued that assimilated observational data may not significantly constrain reanalyses. Nevertheless, our findings support others in the recent literature, and the source terms for the MSE budget equation have a well-established physical basis.

## 5. Exploring connections between CCKWs and TC genesis

So far, we have provided evidence that there is a pronounced influence of convective-radiative feedbacks on TC genesis processes, and that environmental preconditioning could also be important. It follows that convective atmospheric phenomena, such as CCKWs, could affect genesis through these pathways. To address this, we first quantify the statistical relationship between genesis events and CCKWs using our AEW-CCKW database. Then, we expand upon the framework of L22 to investigate how CCKWs modify environmental variables and convection around *developing* AEWs.

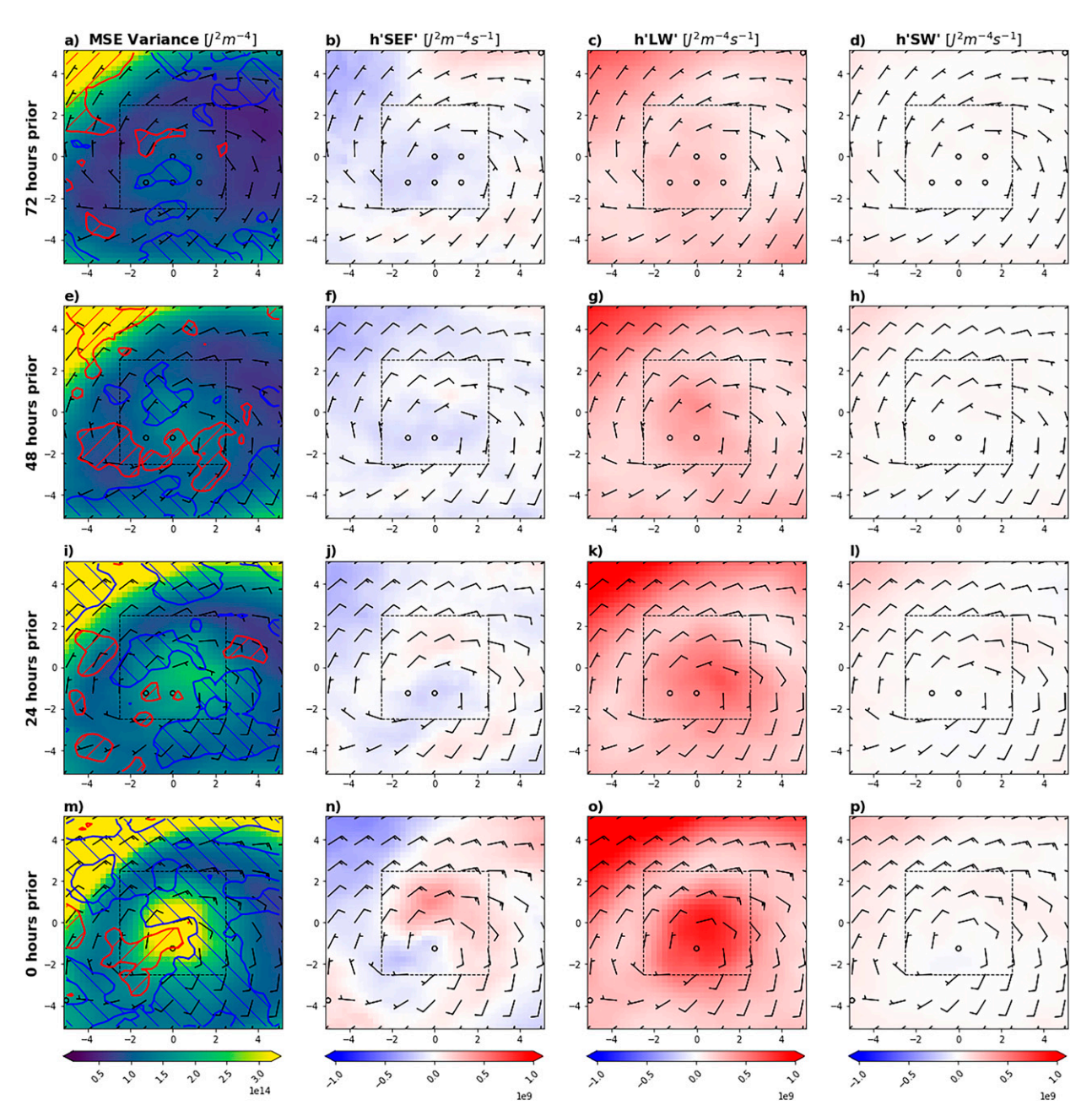
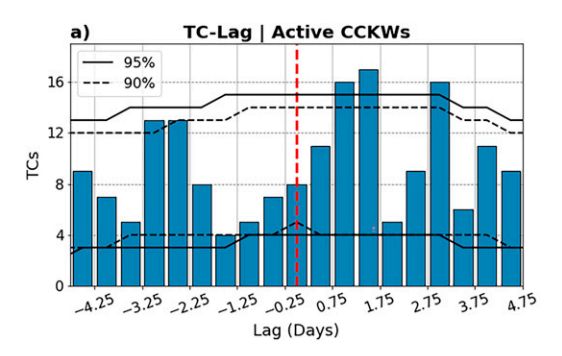


FIG. 7. Composites of MSE variance overlain with (a),(e),(i),(m) the residual; (b),(f),(j),(n) the surface feedback source term; (c),(g),(k),(o) longwave radiative feedback term; and (d),(h),(l),(p) shortwave radiative feedback term in a  $10^{\circ} \times 10^{\circ}$  box surrounding tracked AEWs prior to genesis. The black inner dashed box represents the  $5^{\circ} \times 5^{\circ}$  box used for the averages shown in Fig. 6. These terms are not adjusted for climatology. In (a), (e), (i), and (m) red hatching shows the regions of positive residual values above  $1.5 \times 10^{8} \text{ J}^{2} \text{ m}^{-4} \text{ s}^{-1}$ , and the blue hatching shows regions of negative residual values below  $-1.5 \times 10^{8} \text{ J}^{2} \text{ m}^{-4} \text{ s}^{-1}$ . Wind barbs are for the composite 10-m wind. Times are 72 h prior to genesis in (a)–(d), 48 h prior in (e)–(h), 24 h prior in (i)–(l), and at the time of genesis in (m)–(p). The *x* and *y* axes show the degrees longitude and latitude *relative* to the AEW center. The dashed black box indicates the area of averaging used in Fig. 6.

Finally, we use the logistic regression method of section 3 to identify favorable AEWs and compare those that develop after passing a CCKW with those that do not. This helps isolate the characteristics of AEW-CCKW interactions associated with eventual genesis.

### a. Statistics and climatology

As in previous studies, we will first quantify the lagged relationship between CCKW and TC genesis. Here we define lag as the number of days genesis occurs relative to when its associated AEW passes a CCKW phase; positive



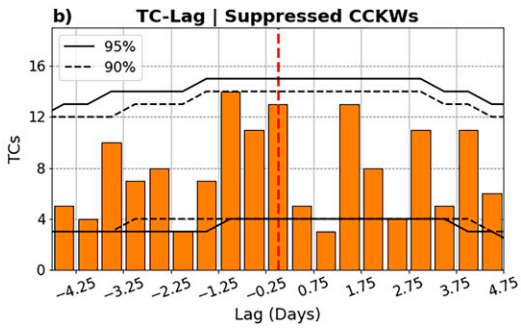


FIG. 8. Number of genesis events, binned in time relative to the center of passing (a) active CCKW phases and (b) suppressed CCKW phases. Horizontal lines: 95% (solid) and 90% (dashed) confidence intervals of genesis occurrences for the expected climatology, discussed in section 2d.

lags indicate genesis occurs after passing the CCKW phase, and vice versa. Genesis events can be associated with multiple CCKW lag times, and thus can show up in multiple bins.<sup>6</sup> The results are compiled separately for active and suppressed CCKW phases (Fig. 8).

There is a statistically significant increase in genesis events 0.75–1.75 days following an active phase of a CCKW (Fig. 8a). Conversely, there is a statistically significant decrease in genesis events 0.75-1.25 days following the suppressed phase of a CCKW (Fig. 8b). While a similar lagged relationship between genesis and active CCKW phases has been shown before (Ventrice et al. 2012a; Schreck 2015), the relationship between the suppressed CCKW phases and genesis is a new result. However, the cause of the significant secondary peak at 2.75–3.25 days for the active lag is unknown. One explanation is noise, given that there is a 5% chance of each bin falling outside the confidence interval by chance. However, we believe these overall results to be robust; not only do they match previous studies, but a test comparing the TC counts between Figs. 8a and 8b (not shown) indicates that the difference in active and suppressed lags for the 0.75-1.25-day lag bin cleared a 99% significance threshold.

The time lag most favorable for genesis after an active CCKW (0.75–1.75 days) is shorter than the 2–3 days found by Schreck (2015). This is likely due to slight differences in methodology. We define the CCKW–TC lag based on the time that a CCKW phase passes an AEW, whereas previous studies define the lag based on when the CCKW passes the longitude of genesis. As the CCKW must travel farther east to encounter the AEW, the spacing between that encounter and genesis is inherently shorter than if the longitude of genesis is used.

It is exceedingly common for AEWs to encounter CCKWs within their lifetimes. Table 1 shows the percentage of AEWs passing at least one active CCKW phase. Notably, up to 76% of all AEWs that result in genesis will pass a CCKW during their lifetime; this fraction drops to 40% when only including encounters over the Atlantic Ocean. The corresponding

fraction for *nondeveloping* AEWs that reach the African coastline are similar. Given the possibility of noise at the 1.0 standard deviation CCKW strength cutoff used in our analysis, these percentages are best considered as an upper limit. Indeed, a smaller percentage of AEWs pass strong (1.5 standard deviation) CCKWs during their lifetimes (Table 1). Nevertheless, these statistics illustrate two important points: that AEW–CCKW passages are common, and that a CCKW encounter does not guarantee genesis will occur. This highlights the importance of understanding why only some AEW–CCKW passages appear to result in genesis.

## b. Characteristics of CCKW encounters for developing AEWs

While L22 explored how CCKWs influence environmental characteristics around nondeveloping AEWs, they excluded AEWs that were associated with TC genesis. Here we build similar composites but *only* include developing AEWs. Like in L22, 600-km averages of AEW-relative environmental fields are computed. All samples at or after the time of genesis are excluded. The compositing point, day 0, corresponds to the time an AEW is collocated in longitude with an active CCKW phase.

Unsurprisingly, a similar pattern emerges for developing AEWs as was shown by L22 for nondeveloping AEWs. While the relative vorticity signal is a bit muddied (Fig. 9a), there is a clear increase in specific humidity surrounding the AEW (Fig. 9b): first in the lower troposphere (1000–700 hPa) prior to the active CCKW passage, and then expanding to the middle and upper troposphere (700–250 hPa). Specific humidity values are elevated for up to 1.5 days following the active CCKW passage. There is also an increase in diabatic heating (Fig. 9c) occurring in phase with the active CCKW passage. Opposite signed deviations before and after the active CCKW (i.e., at -1 day; +1 day) are likely associated with the suppressed phase that typically surrounds an active phase.

An eastward filter may better exclude AEW-related variability and reveal contributions from the Kelvin wave band, as demonstrated by the eastward-filtered composite of relative vorticity (Fig. 9d). This filter is computed identically to the one used in Lawton et al. (2022). This composite illustrates a significant increase in vorticity at low levels collocated

<sup>&</sup>lt;sup>6</sup> Cases falling into multiple bins represent only a small fraction of binned events, and sensitivity testing using various methods of exclusion resulted in similar results.

TABLE 1. The percentage of AEWs that pass at least one active CCKW phase. Results using CCKW strength thresholds of 1.0 and 1.5 standard deviation are shown. Nondevelopers are subdivided into all AEWs and those AEWs reaching the coastline (18°W). Developers are subdivided into categories based on the lag between the CCKW passage and genesis. By definition, a CCKW passage must occur prior to genesis to be counted. The right-hand column denotes the percentage of AEWs with CCKW passage occurring at or west of 20°W.

		Any	At or west of 20°W (%) 1.0 std dev	
Category		1.0 std dev		1.5 std dev
Nondevelopers	All	57.9	32.0	50.5
	Those reaching coastline	71.9	41.6	_
Developers	All	76.3	34.4	40.0
	0–3-day lag	48.1	15.6	33.3
	0–2-day lag	33.1	10.0	26.0
	0.75–1.75-day lag	20.6	6.9	16.0

with the active CCKW passage, quickly shifting to the middle-troposphere and persisting for up to 2 days afterward. Meanwhile, a similar pattern to that of the full composites is seen in the eastward-filtered plots of specific humidity and diabatic heating (Figs. 9e,f). There are not significant differences of note for westward-filtered versions of these composites.

Next, we address how these environmental changes may connect to the time-lagged relationship between CCKWs and genesis (Fig. 8a; Ventrice et al. 2012a; Schreck 2015). New CCKW-relative composites are created that include AEWs for which a statistical relationship between CCKWs and genesis has been found: the 0.75–1.75-day window after an active CCKW passage (Fig. 10). The resulting composite contains 33 samples. Convective coverage (Fig. 10a) and diabatic heating (Fig. 10b) initially increase in phase with the active CCKW passage and remain elevated above climatology throughout most of the composite. Trends in the total column

water vapor (Fig. 10c) and specific humidity (Fig. 10d) follow a similar pattern; specific humidity elevates above climatology in the lower troposphere beginning a day prior to the active CCKW, with increases in the upper levels following shortly after. Composites of relative vorticity, meanwhile, did not demonstrate significant increases until about +0.5 days after the active CCKW (not shown).

These composites resemble an amalgamation of the standalone CCKW-relative composites (Fig. 9) and the genesis-relative composites discussed earlier (Fig. 5). In fact, the overlap of CCKW- and genesis-related signals can be evidenced by breaking down these composites into their eastward- and westward-propagating components (Fig. 11). An enhancement in eastward-propagating diabatic heating, likely driven by CCKWs, is clear beginning at 0.5 days prior to the CCKW and lasting 0.75 days afterward (Fig. 11a). Its westward-propagating counterpart—which may include contributions from

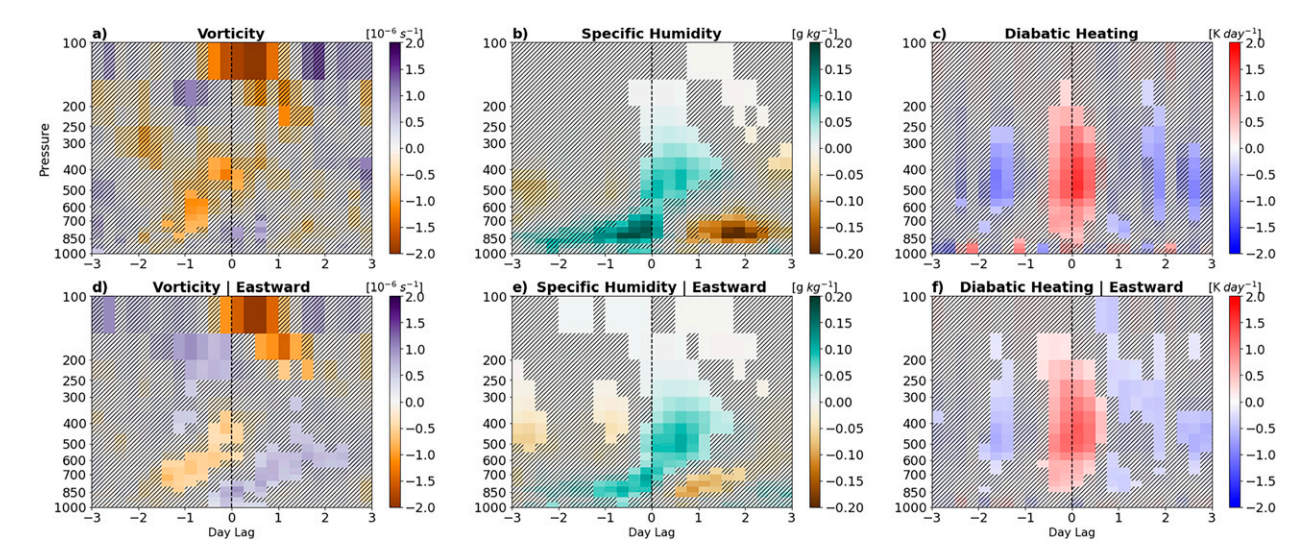


FIG. 9. CCKW-relative composites of environmental variables averaged within 600 km of developing AEWs. Values are deviations from the longitudinal climatology of developing AEWs. Unfiltered plots are of (a) relative vorticity, (b) specific humidity, and (c) diabatic heating (Q1) around the active phase of CCKWs. (d)–(f) As in (a)–(c), but with only the eastward-propagating part of the signal retained. Day 0 is defined as when an AEW is aligned in longitude with the active phase of a CCKW. Regions that are not statistically significant at a 95% threshold are hatched out; significance is evaluated for null hypothesis 1. Composites are also normalized relative to the mean bootstrapped climatological value at each time lag.

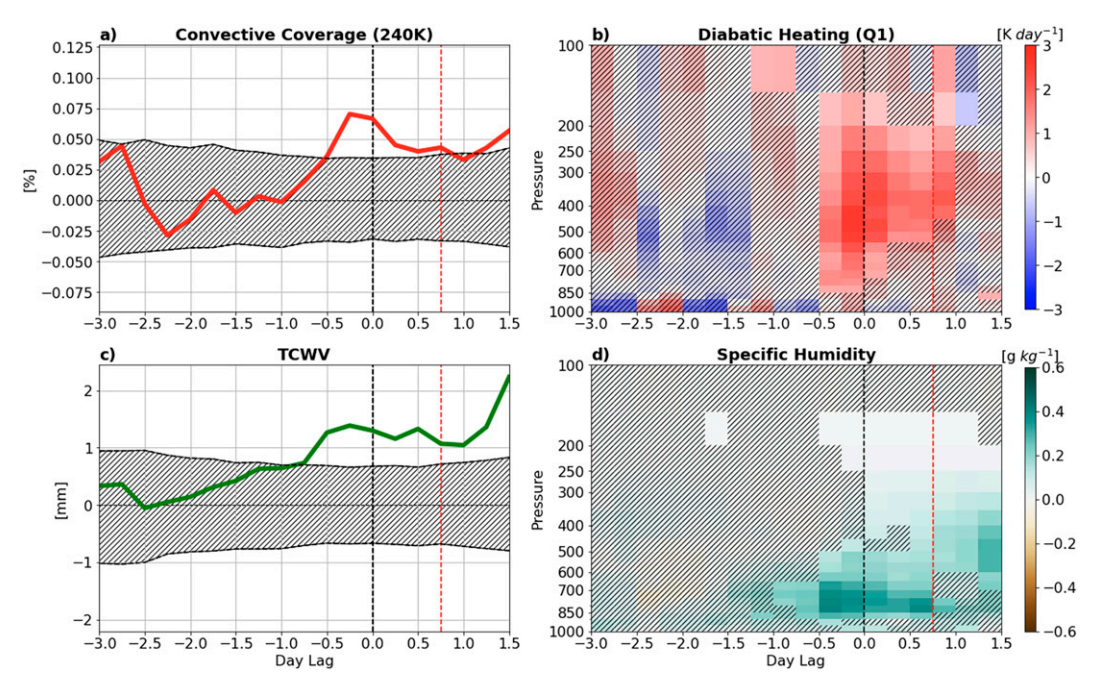


FIG. 10. Similar CCKW-relative composites to Fig. 9, but only including *developing AEWs* that result in genesis within 0.75–1.75 days of an active CCKW passage (vertical dashed black line). Displayed fields include (a) convective coverage using a 240-K threshold, (b) diabatic heating, (c) TCWV, and (d) specific humidity. A bootstrapping technique (null hypothesis 1) is used to generate the 95% confidence interval of the background climatology; for single-level plots this interval is displayed as a filled hatched region in (a) and (c), and for multiple-level plots in (b) and (d), areas that do *not* clear significance are hatched out. AEW samples are only included in the composite if they occur prior to genesis—the red vertical dashed line indicates the earliest time lag at which genesis can occur (+0.75 days).

the AEW itself, MCSs, offshore propagating convection, and more-looks similar, although it slightly shifted to later time lags (Fig. 11b). Contributions from specific humidity are more varied. Increases in eastward propagating specific humidity are concentrated in the middle and upper troposphere (Fig. 11c), whereas the westward-propagating signal begins earlier and primarily in the lower troposphere (Fig. 11d). This implies that CCKWs could: 1) directly contribute to the enhancement of convection in the vicinity of an AEW prior to genesis and 2) directly moisten the middle and upper troposphere, helping bring these regions closer to saturation. However, it is not possible to confirm a causal link here: although the CCKW is modifying these terms prior to genesis, it does not directly imply that these changes were necessary for genesis to proceed. Nevertheless, these results raise the possibility that the CCKW-related environmental changes could be serving as an initiator of the genesis processes discussed in section 4, either by bringing the column closer to saturation or by encouraging convective aggregation through the enhancement of preexisting convective activity. The sequence of events shown in Fig. 10 is congruent with such a hypothesis: with CCKW-relative anomalies beginning roughly 0.5 days prior to the CCKW passage, a typical 2-day incubation period (the timeframe shown in Fig. 5 and previous work) would result in genesis occurring 1.5 days after the active CCKW passage. This is within the 0.75–1.75-day window of Fig. 8, perhaps not by coincidence.

### c. Differentiating characteristics that result in TC genesis

We now attempt to quantify characteristics of AEW–CCKW passages that differentiate whether or not they result in TC genesis. Such an analysis addresses two important goals. First, it may have operational implications for predicting the outcome of AEW–CCKW passages in real time. Second, it may provide insight into which environmental factor(s) serve as a link between the large-scale CCKW modifications and genesis processes.

First, we use the logistic regression results at 20°W to define favorable AEWs (section 3) and remove AEW–CCKW passages for unfavorable waves from our comparison. This is necessary to reduce the impact of weak, unimportant AEWs that dominate the nondeveloping sample. Some additional restrictions are then placed on each sample set; all AEW–CCKW passages must occur between 40°–10°W and 5°–20°N, and genesis for the developing sample set must occur 0.75–1.75 days after the AEW–CCKW passage. This analysis was repeated with TC genesis lag bounds of 0–2, 0–3, 1–2, and 1–3 days, with no appreciable impact on the results. The final locations of our included samples and associated statistics are shown in Fig. 12. Note that there are over 4 times more nondeveloping passages than developing passages, highlighting the scarcity of genesis events relative to the number of AEWs that move off the African coastline.

There is not a noticeable difference in the strength of passing CCKWs (as measured by the  $0^{\circ}$ – $10^{\circ}$ N average of Kelvin-filtered  $T_b$ ) for passages that are associated with genesis versus those that do not (Fig. 12b). The longitude of the developing AEW cases

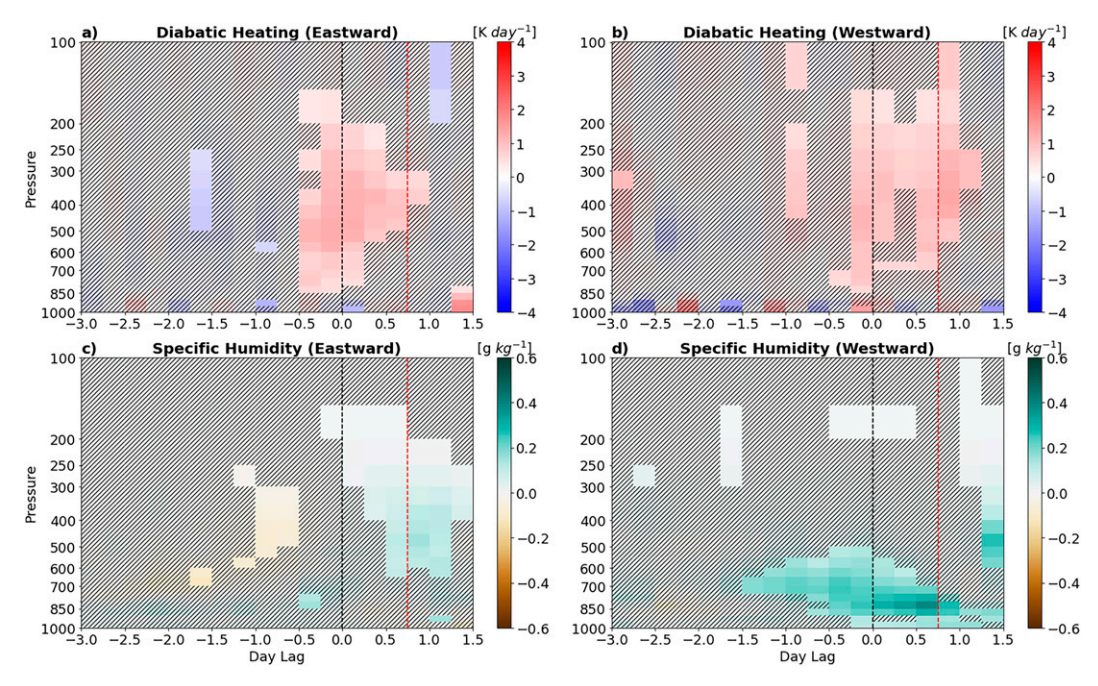


FIG. 11. (a),(b) As in Fig. 10b, but only using the eastward- and westward-propagating components of the diabatic heating signal, respectively. (c),(d) As in Fig. 10d, but only using the eastward- and westward-propagating components of the specific humidity signal, respectively.

was also shifted to the east relative to nondevelopers (Fig. 12c), which could partially be an artifact of our selected domain. However, using a 30°W western boundary instead of 40°W does not dramatically change the results presented later in this section. Developing cases have AEWs located more equatorward during the CCKW passage compared with nondeveloping cases (Fig. 12d). This is partially explained by the typical climatological pattern of developing versus nondeveloping AEWs (not shown). However, it may also suggest that the AEWs are closer to the CCKW envelope in these scenarios, potentially enhancing their interactions.

Even more stark differences arise when comparing environmental fields (Fig. 13). Convective coverage (Fig. 13b) and diabatic heating (Fig. 13e) appear to be the clearest differentiators for passages that result in genesis. For the developing cases, convective activity is significantly elevated relative to nondeveloping cases near the time of CCKW passage (from -0.25- to 0-day lag), with a secondary peak +0.5 days after the CCKW passage. Other terms, such as TCWV (Fig. 13a), 200–850-hPa wind shear magnitude (Fig. 13c), and specific humidity (Fig. 13d) do not have significantly higher for the developing cases, but only starting 0.5 days after the active CCKW phase and seemingly limited to the lower troposphere.

These composites are also broken down into their eastward-and westward-propagating components, with select results shown in Fig. 14. While there are no apparent differences in the eastward-propagating diabatic heating term (Fig. 14a), there *are* significant differences in the westward-propagating part of the signal (Fig. 14b). In other words, the higher absolute values of diabatic heating noted for developers in Fig. 13e appear to be driven by changes in westward-propagating convection, not the eastward-propagating signal associated with CCKWs. A similar pattern is also apparent in the filtered specific humidity (Figs. 14c,d); developing cases tend to have higher values of westward-propagating upper-level humidity (350–200 hPa) during and after the CCKW passage as compared to nondeveloping cases. This pattern in upper-level humidity is likely tied to the noted changes in convection.

Similar composites can be built for the MSE variance source terms explored in section 4 (Fig. 15). Comparisons between developing and nondeveloping cases show elevated MSE variance and longwave-radiative feedbacks in a 0-1-day window following the active CCKW passage (Figs. 15a,b) for the developing cases. A more modest difference is also seen in the surface feedback fields, but it is not significant (Fig. 15c). CCKWs increase convective coverage and diabatic heating around AEWs prior to genesis (Figs. 10 and 11), and if this were to preferentially occur where convection already exists (i.e., around the AEW), it could theoretically drive a convectiveradiative feedback. However, it is also possible the differences seen in Fig. 15b are simply artifacts of the concurrence of genesis in these plots. Asserting a more direct connection is not possible in this framework and requires more detailed attribution work in the future. For now, we argue that the

<sup>&</sup>lt;sup>7</sup> The main difference is a slightly reduced extent of statistical significance for convective coverage and diabatic heating composites when using the 30°W western boundary. This is likely driven by a reduced sample of 15 developing cases and 53 nondeveloping cases, making the 95% significance threshold harder to clear.

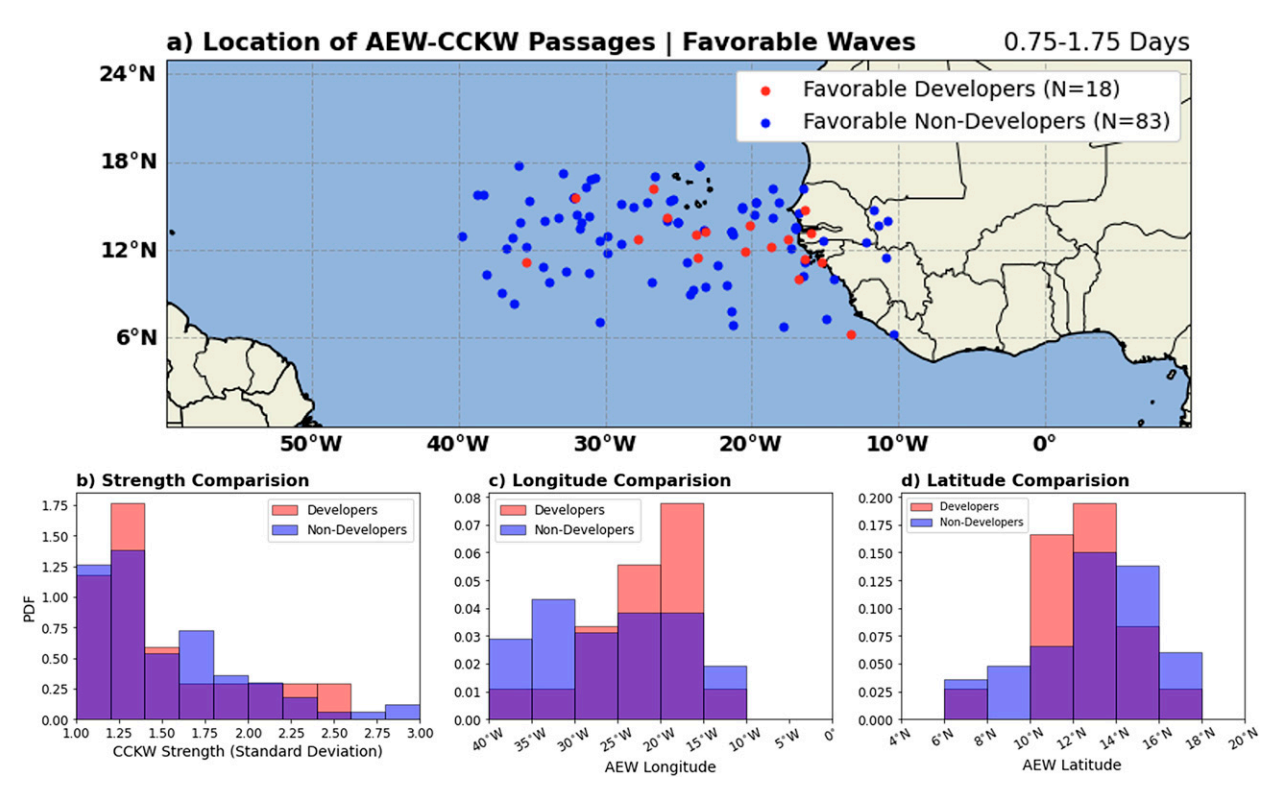


FIG. 12. General characteristics of AEW-CCKW passages for AEWs classified as "favorable" by the logistic regression run at 20°W. (a) The location of the AEW for each AEW-CCKW passage, classified as either developing (red) or nondeveloping (blue). (b) The PDF of CCKW strength, as measured by the  $0^{\circ}$ - $10^{\circ}$ N average of Kelvin-filtered  $T_b$  at the longitude of the tracked AEW during the passage. (c),(d) As in (b), but for the AEW's longitude and latitude, respectively.

existence of a CCKW-genesis relationship implies at least an indirect relationship to convective aggregation and its sources.

Finally, we consider whether genesis proceeds differently while under the influence of a CCKW. To do so, we compare genesis-relative composites of those cases likely influenced by CCKWs (0.75–1.75-day lag window) to that of other genesis

cases (Fig. 16). We note two primary differences. For one, the increase in convection-associated diabatic heating (Figs. 16a,b) and convective coverage (not shown) is slightly delayed for the CCKW-related cases, with an enhancement around the time of the active CCKW phase passage (within black vertical lines) versus typical genesis events. This could reflect the

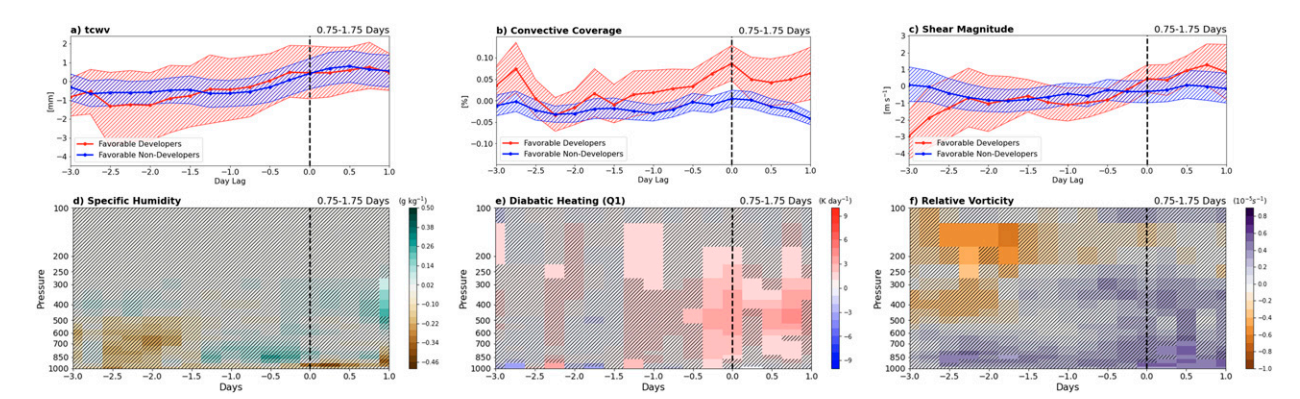


FIG. 13. CCKW-relative composites (600-km averaging radius) comparing AEW-CCKW passages that result in genesis vs those that do not. In the single-level comparisons of (a) TCWV, (b) convective coverage (percent within 600 km), and (c) 200-850-hPa vertical wind shear, the 95% confidence interval is hatched around each composite average. Data for developing cases are shaded red and data for non-developing cases are shaded blue. For the multiple-level plots of (d) specific humidity, (e) diabatic heating, and (f) relative vorticity averages, we plot the *difference* between developing and nondeveloping cases. Regions that are *not* significantly different at a 95% threshold are hatched out. Here we test null hypothesis 2 using a bootstrapping method, as defined in the methodology.

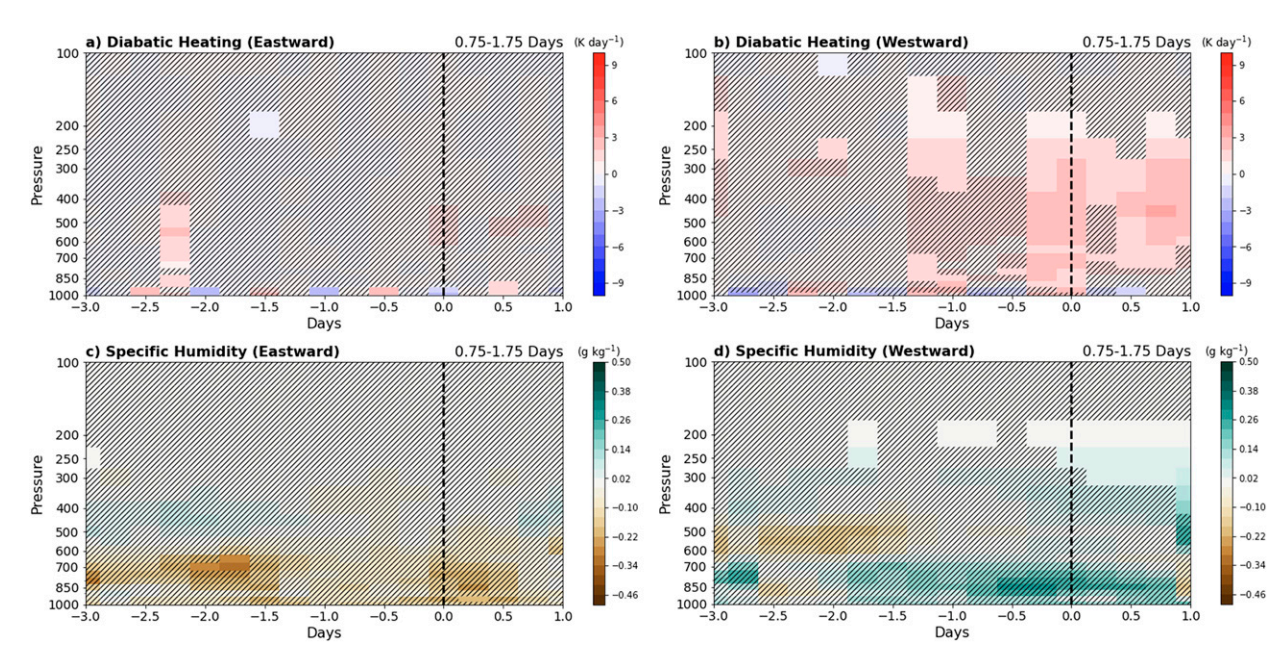


FIG. 14. (a),(b) As in Fig. 13e, but using the eastward- and westward-propagating components of the diabatic heating signal, respectively. (c),(d) As in Fig. 13d, but using the eastward- and westward-propagating components of the specific humidity signal, respectively.

impact of the commonly preceding suppressed CCKW phase in limiting convection 2–3 days prior to genesis. Second, the development of an upper-level anticyclone is more pronounced for events associated with CCKWs (Figs. 16e,f), especially in the 2-day window prior to genesis. This supports previous work suggesting that CCKWs could provide a more favorable upper-level environment and enhanced outflow for genesis (Schreck 2016; L22). However, despite these observed differences, the overall progression of environmental fields is similar with or without the presence of a CCKW. While CCKWs are likely influencing the onset and favorability of genesis, there is not any overwhelming evidence that genesis proceeds differently once initiated.

### 6. Discussion and conclusions

In this work, we used a 39-yr database of AEWs and CCKWs to investigate the connections between TC genesis and CCKWs in ERA5 and GridSat-B1 data. AEWs were objectively classified as favorable or unfavorable to genesis using a logistic regression algorithm, with inputs tested from a range of longitudes (40°W–30°E). This model shows significant skill

in diagnosing AEW favorability as far east as central Africa, illustrating that AEW characteristics over the African continent can be predictive of their development well downstream. This is in line with several studies indicating that AEW attributes over West Africa (Hopsch et al. 2010; Agudelo et al. 2011) and environmental characteristics over East Africa (Núñez Ocasio et al. 2021) are tied to AEW outcomes over the Atlantic.

Composites of genesis support previous hypotheses on the role of environmental preconditioning and radiative–convective feedbacks in the genesis process. Reanalysis data indicates that TC genesis takes several days to complete, with convective coverage, associated diabatic heating, and column specific humidity all significantly elevated more than 2 days prior to the official genesis time in HURDAT. This is consistent with the 2-day moistening trend Zawislak and Zipser (2014) found using dropsonde data and the increase in convection and precipitation coverage shown by Leppert et al. (2013a,b) and Zawislak (2020). It also supports the theory of environmental preconditioning suggested in previous studies (e.g., Davis 2015; Nolan 2007). Meanwhile, a composited MSE spatial variance budget demonstrates an increase in

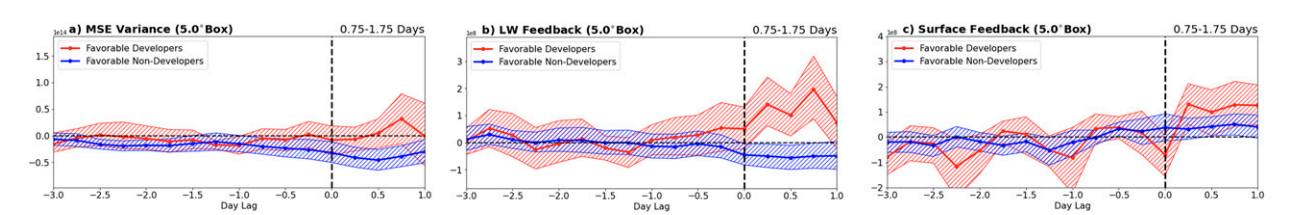


FIG. 15. As in Figs. 13a-c, but comparing (a) MSE variance, (b) longwave-radiative feedback, and (c) surface feedback between developing and nondeveloping AEW-CCKW passages. Values are adjusted for the AEW climatology in longitude.

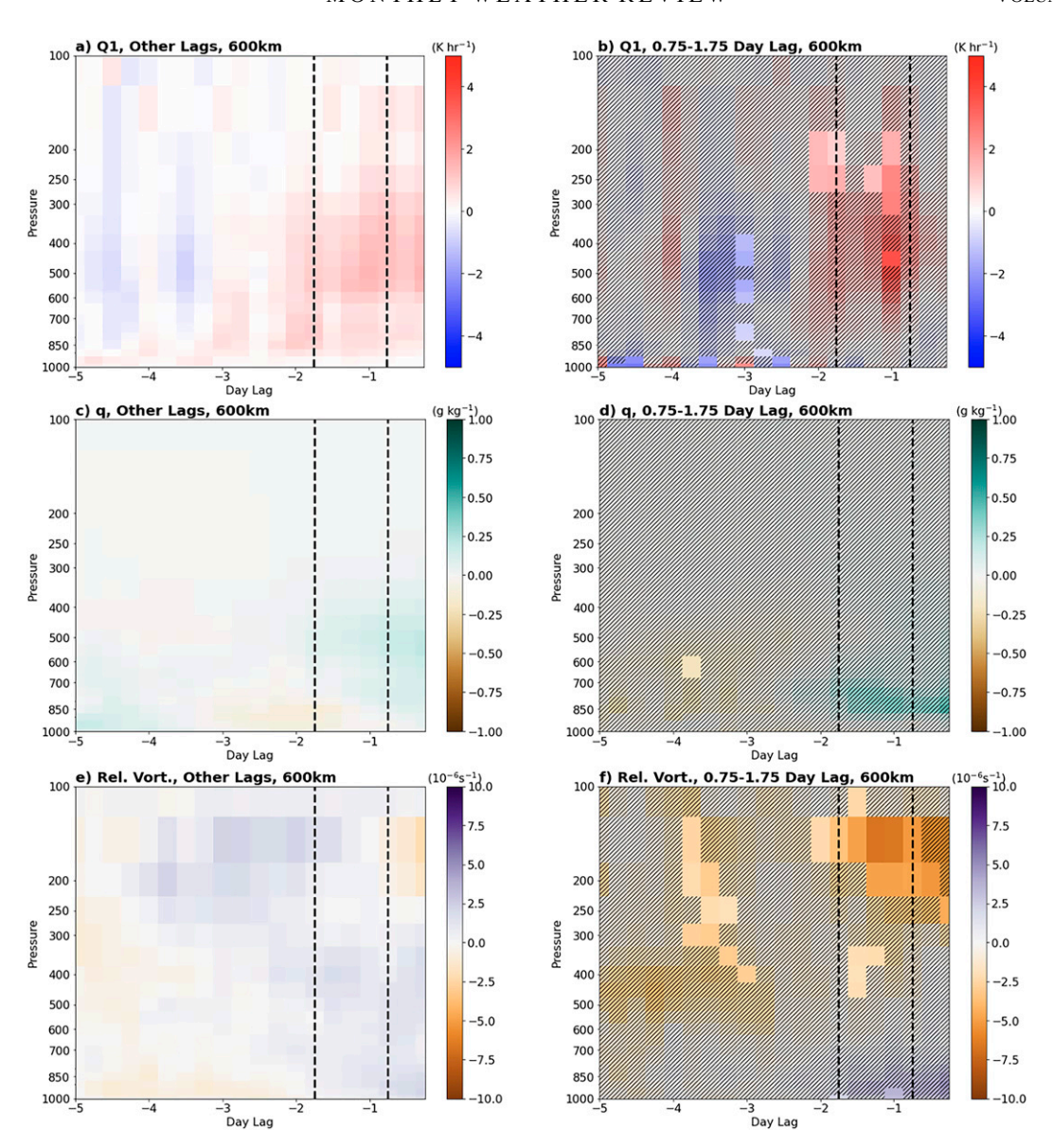


FIG. 16. Genesis-relative composites of (a),(b) diabatic heating; (c),(d) specific humidity; and (e),(f) relative vorticity. The indicated lag time is relative to genesis, which occurs at the right side of each composite. (left) Only includes samples either *outside* the 0.75–1.75-day lag window or without CCKW passages at all, whereas (right) only includes samples *within* this 0.75–1.75-day lag window. The two vertical dashed black lines indicate the window of time when the active CCKW passage occurs in the 0.75–1.75-day lag window cases. Areas where the two composites are *not* significantly different at a 95% threshold are hatched out in the right panels only.

MSE variance (a proxy for convective aggregation) that begins roughly two days prior to genesis, driven primarily by longwave radiative feedbacks. These feedbacks may enhance the radial gradient of heating, promoting a transverse circulation that converges humidity and angular momentum. Our results suggest that surface feedbacks only become relevant to genesis later in the process when surface wind speeds are strong enough to promote efficient ocean—atmosphere enthalpy exchange. These results are congruent with similar MSE variance budgets computed for genesis and intensification in various modeling frameworks

(Carstens and Wing 2020; Ruppert et al. 2020; Wu et al. 2021; Wing 2022) and reanalysis (Dirkes et al. 2023). However, these results are limited by our use of a single reanalysis dataset (ERA5) and potential errors in the representation of genesis processes in reanalysis data (Dirkes et al. 2023; our section 4). More work is also needed to quantify how genesis processes are represented across different reanalysis datasets. Nevertheless, convective aggregation and environmental preconditioning are both plausible pathways by which CCKWs and other phenomenon could directly impact the TC genesis process.

An analysis of CCKW-centered composites suggests that modifications to convection and moisture could be one pathway that these waves influence tropical cyclogenesis. CCKW passages are common, with over 70% of all AEWs passing at least one CCKW in their lifetimes. As in previous studies (Ventrice et al. 2012a; Schreck 2015), we find a statistically significant increase in genesis events in a 0.75-1.75-day window following the passage of the active phase of a CCKW. We also show that the opposite is true for the convectively suppressed phase, which temporarily inhibits genesis. As shown in previous studies (e.g., Ventrice et al. 2012b; Schreck 2016; L22), active CCKW phases temporarily increase moisture and convective activity in the days leading up with genesis. We find that convective coverage and diabatic heating at the time of CCKW passage are the main discriminators between AEW-CCKW interactions that result in genesis versus those that do not. However, once initiated, the progression of genesis is generally similar with or without the influence of a CCKW. Given these results, the convective response of AEWs to CCKWs should be monitored in real time as an indicator of potential TC development.

This study provides evidence that CCKW-driven modifications to convection and humidity could play a role in preconditioning AEWs and enhancing radiative-convective feedbacks. However, determining a causal relationship between CCKWs and genesis processes is challenging using this framework. It is still unclear if CCKWs are modifying the overall climatology of genesis events, or simply impacting the *timing* of genesis. This motivates further investigation of AEW-CCKW interactions in numerical simulations, where experiments more suited to investigate cross-scale interactions and causality can be run.

While our results suggest that moisture and convection could serve as an important aspect of the TC-CCKW relationship, this does not exclude other previously identified factors from playing a role. For example, enhanced AEW-relative recirculation induced by CCKWs (Schreck 2016; L22), increased upper-level outflow (Schreck 2016; L22; Fig. 16f), and modifications to vertical wind shear (Ventrice et al. 2012b; L22), all have the potential to increase the likelihood of genesis and can indirectly modify convection and moisture. As TC favorability is the combination of many factors, the specific influence of CCKWs may vary on a case-by-case basis.

Acknowledgments. This project was funded by NSF Grant AGS-1747781 and through an NSF Graduate Research Fellowship (1938060). We are grateful to Alexis Wilson, Allison Wing, Jarrett Starr, and Rosimar Rios-Berrios for helpful discussions that substantially improved this manuscript. We also thank Carl Schreck and an anonymous reviewer for helpful feedback on the paper.

Data availability statement. Objective AEW tracks and CCKW positions used in this study are publicly available in a repository at https://doi.org/10.17605/OSF.IO/J4HPQ. ERA5 data were obtained via the Copernicus Climate Data Store at http://cds.climate.copernicus.eu (Hersbach et al. 2020). GridSat-B1 satellite data were obtained from https://www.ncdc.noaa.gov/gridsat/gridsat-index.php (Knapp et al. 2011).

#### **APPENDIX**

### Application of Logistic Regression to AEWs

In this work, we apply a logistic regression model similar to that of Brammer and Thorncroft (2015) to estimate each AEW's favorability to TC genesis. To perform these regressions, we leverage the Scikit-learn python package and its corresponding mathematical definitions (Pedregosa et al. 2011; Scikit-learn 2022a). Logistic regression is a simple machine learning technique that uses input data to train a linear model to predict binary outcomes. Once established, this predictive model computes a probability score p (which we refer to as a "favorability score") for each AEW. Favorability scores estimate the probability that a given AEW will undergo TC genesis and can range from 0 to 1. A set threshold of p = 0.5 is then used for binary classification: AEWs with a score below this value are considered "unfavorable" for TC genesis, while AEWs with scores at or above this value are considered "favorable" for TC genesis. The threshold of p = 0.5 was chosen for consistency with Brammer and Thorncroft (2015). Mathematically, the favorability score p is defined by Scikit-learn (2022a) as follows:

$$p(t) = \frac{1}{1 + e^{-t}},\tag{A1}$$

where t in (A1) is represented by

$$t(X_n) = \beta_0 + \beta_1 X_1 + \beta_2 X_2 + \dots + \beta_n X_n.$$
 (A2)

In Eq. (A2),  $X_n$  represents the input data ("predictors") and  $\beta_n$  represents their corresponding coefficients. A logistic regression model determines these coefficients by minimizing a cost function using samples with known binary outcomes (Scikit-learn 2022a). In the case of AEWs, the input data consists of selected AEW or environmental attributes, and the binary outcome is whether TC genesis occurs. While categories of input data with larger absolute coefficients will weigh more heavily on the predictive score than others, it is ultimately the linear combination of these terms that determines the final favorability score.

To apply this method to AEW favorability, we train separate logistic regression models based on longitude, which are spaced apart every 10° from 40°W to 30°E. As discussed in section 2b, predictors consist of environmental fields averaged within 500 km of the AEW along with other wave attributes. These data are standardized prior to use in the model. Each included AEW is assigned a binary outcome value of 0 or 1, which indicates if TC genesis occurs at or east of 40°W. This longitude restriction is loosened for ocean-based regressions, where genesis simply must occur within 20° of the input longitude. AEWs that undergo genesis west of a longitude threshold are excluded from the regression entirely. To reduce overfitting, AEWs are randomly sorted such that only 70% of cases are used for training the model, though all cases are included for final diagnostics. Finally, since the binary outcomes are imbalanced (there are significantly more nongenesis events than genesis events),

TABLE A1. List of all potential input variables for the logistical regression models, with those selected in the final model at 20°W italicized. The normalized coefficient values for the 20°W logistic regression are also shown in the right column.

Category	Variable names	Coefficient for 20°W input
AEW climatological attributes	Julian day of year	0.90
_	Days AEW has existed	_
	Latitude of AEW	_
Environmental averages at single level	850-hPa temperature	1.33
	850-hPa relative vorticity	0.74
	850-hPa specific humidity	1.30
	400-hPa relative vorticity	<del>_</del>
	400-hPa specific humidity	_
Multilevel averages or proxy fields	Convective coverage around AEW	0.62
	200-300-hPa average divergence	0.51
	400-700-hPa average specific humidity	_
	300–800-hPa average vertical velocity	_
	200–850-hPa wind shear	_

the cost function is weighted based on outcome frequency. This penalizes mistakes in the TC genesis outcome more; otherwise, simply classifying *every* AEW as an unfavorable wave would erroneously suggest high model skill.

As discussed by Brammer and Thorncroft (2015), using too many predictors could overfit the logistic regression. Furthermore, using highly correlated predictors (i.e., humidity at 500 and 700 hPa) could reduce the overall skill of the model. We carefully selected our predictors to be representative of fields associated with TC genesis, typical AEW variability, and AEW-CCKW interactions (Brammer and Thorncroft 2015; Lawton et al. 2022). Additionally, we conducted a series of sensitivity tests using various environmental parameters. While these tests are generally consistent with one another, the variables listed in Table A1 result in the highest skill for our logistic regression models. Additionally, we apply recursive feature elimination (RFE; Scikit-learn 2022b) to reduce the number of predictors to six prior to training the logistic regression models. RFE iteratively considers fewer and fewer features until six remain, eliminating the least important feature during each iteration. This is done separately at each input longitude.

To provide a tangible example of the logistic regression output, coefficients found using the 20°W logistic regression are provided in Table A1. AEWs at 20°W with higher values of 850-hPa vorticity, temperature, and specific humidity are more likely to result in genesis, and thus these parameters have positive coefficients from the logistic regression (Table A1). The same is true of AEWs with increased convective coverage and greater upper-level divergence at this longitude. Because RFE is run separately at each input longitude, logistic regression models at other longitudes can, and do, utilize different predictors.

### REFERENCES

Agudelo, P. A., C. D. Hoyos, J. A. Curry, and P. J. Webster, 2011: Probabilistic discrimination between large-scale environments of intensifying and decaying African easterly waves. *Climate Dyn.*, 36, 1379–1401, https://doi.org/10.1007/ s00382-010-0851-x. Berry, G. J., and C. D. Thorncroft, 2012: African easterly wave dynamics in a mesoscale numerical model: The upscale role of convection. J. Atmos. Sci., 69, 1267–1283, https://doi.org/10. 1175/JAS-D-11-099.1.

Bian, G.-F., G.-Z. Nie, and X. Qiu, 2021: How well is outer tropical cyclone size represented in the ERA5 reanalysis dataset? *Atmos. Res.*, 249, 105339, https://doi.org/10.1016/j.atmosres. 2020.105339.

Brammer, A., and C. D. Thorncroft, 2015: Variability and evolution of African easterly wave structures and their relationship with tropical cyclogenesis over the eastern Atlantic. *Mon. Wea. Rev.*, 143, 4975–4995, https://doi.org/10.1175/MWR-D-15-0106.1.

—, —, and J. P. Dunion, 2018: Observations and predictability of a nondeveloping tropical disturbance over the eastern Atlantic. *Mon. Wea. Rev.*, **146**, 3079–3096, https://doi.org/10.1175/MWR-D-18-0065.1.

Burpee, R. W., 1972: The origin and structure of easterly waves in the lower troposphere of North Africa. *J. Atmos. Sci.*, **29**, 77–90, https://doi.org/10.1175/1520-0469(1972)029 <0077:TOASOE>2.0.CO;2.

Cangialosi, J. P., 2022: National Hurricane Center forecast verification report: 2021 hurricane season (25 April 2022). NOAA/ National Hurricane Center, 76 pp., https://www.nhc.noaa.gov/ verification/pdfs/Verification\_2021.pdf.

——, E. Blake, M. DeMaria, A. Penny, A. Latto, E. Rappaport, and V. Tallapragada, 2020: Recent progression in tropical cyclone intensity forecasting at the National Hurricane Center. Wea. Forecasting, 35, 1913–1922, https://doi.org/10.1175/WAF-D-20-0059.1.

Carstens, J. D., and A. A. Wing, 2020: Tropical cyclogenesis from self-aggregated convection in numerical simulations of rotating radiative-convective equilibrium. J. Adv. Model. Earth Syst., 12, e2019MS002020, https://doi.org/10.1029/2019MS002020.

Chien, M.-T., and D. Kim, 2023: Representation of the convectively coupled Kelvin waves in modern reanalysis products. J. Atmos. Sci., 80, 397–418, https://doi.org/10.1175/JAS-D-22-0067.1

Davis, C. A., 2015: The formation of moist vortices and tropical cyclones in idealized simulations. *J. Atmos. Sci.*, **72**, 3499– 3516, https://doi.org/10.1175/JAS-D-15-0027.1.

Dirkes, C. A., A. A. Wing, S. J. Camargo, and D. Kim, 2023: Process-oriented diagnosis of tropical cyclones in reanalyses

- using a moist static energy variance budget. *J. Climate*, https://doi.org/10.1175/JCLI-D-22-0384.1, in press.
- Fritz, C., Z. Wang, S. W. Nesbitt, and T. J. Dunkerton, 2016: Vertical structure and contribution of different types of precipitation during Atlantic tropical cyclone formation as revealed by TRMM PR. *Geophys. Res. Lett.*, 43, 894–901, https://doi.org/10.1002/2015GL067122.
- Gruber, A., 1974: The wavenumber-frequency spectra of satellite-measured brightness in the tropics. *J. Atmos. Sci.*, **31**, 1675–1680, https://doi.org/10.1175/1520-0469(1974)031<1675: TWFSOS>2.0.CO;2.
- Hall, N. M. J., G. N. Kiladis, and C. D. Thorncroft, 2006: Threedimensional structure and dynamics of African easterly waves. Part II: Dynamical modes. J. Atmos. Sci., 63, 2231– 2245, https://doi.org/10.1175/JAS3742.1.
- Hersbach, H., and Coauthors, 2020: The ERA5 global reanalysis. *Quart. J. Roy. Meteor. Soc.*, **146**, 1999–2049, https://doi.org/10.1002/qj.3803.
- Hopsch, S. B., C. D. Thorncroft, and K. R. Tyle, 2010: Analysis of African easterly wave structures and their role in influencing tropical cyclogenesis. *Mon. Wea. Rev.*, 138, 1399–1419, https:// doi.org/10.1175/2009MWR2760.1.
- Jones, E., A. A. Wing, and R. Parfitt, 2021: A global perspective of tropical cyclone precipitation in reanalyses. *J. Climate*, 34, 8461–8480, https://doi.org/10.1175/JCLI-D-20-0892.1.
- Kiladis, G. N., C. D. Thorncroft, and N. M. J. Hall, 2006: Threedimensional structure and dynamics of African easterly waves. Part I: Observations. J. Atmos. Sci., 63, 2212–2230, https://doi.org/10.1175/JAS3741.1.
- —, M. C. Wheeler, P. T. Haertel, K. H. Straub, and P. E. Roundy, 2009: Convectively coupled equatorial waves. *Rev. Geophys.*, 47, RG2003, https://doi.org/10.1029/2008RG000266.
- Knapp, K. R., and Coauthors, 2011: Globally gridded satellite observations for climate studies. *Bull. Amer. Meteor. Soc.*, 92, 893–907, https://doi.org/10.1175/2011BAMS3039.1.
- Komaromi, W. A., 2013: An investigation of composite dropsonde profiles for developing and nondeveloping tropical waves during the 2010 PREDICT field campaign. J. Atmos. Sci., 70, 542–558, https://doi.org/10.1175/JAS-D-12-052.1.
- Landsea, C. W., and J. L. Franklin, 2013: Atlantic hurricane database uncertainty and presentation of a new database format. *Mon. Wea. Rev.*, 141, 3576–3592, https://doi.org/10.1175/ MWR-D-12-00254.1.
- Lawton, Q. A., S. J. Majumdar, K. Dotterer, C. Thorncroft, and C. J. Schreck III, 2022: The influence of convectively coupled Kelvin waves on African easterly waves in a wave-following framework. *Mon. Wea. Rev.*, 150, 2055–2072, https://doi.org/ 10.1175/MWR-D-21-0321.1.
- Leppert, K. D., II, D. J. Cecil, and W. A. Petersen, 2013a: Relation between tropical easterly waves, convection, and tropical cyclogenesis: A Lagrangian perspective. *Mon. Wea. Rev.*, 141, 2649–2668, https://doi.org/10.1175/MWR-D-12-00217.1.
- ——, W. A. Petersen, and D. J. Cecil, 2013b: Electrically active convection in tropical easterly waves and implications for tropical cyclogenesis in the Atlantic and east Pacific. *Mon. Wea. Rev.*, **141**, 542–556, https://doi.org/10.1175/MWR-D-12-00174.1.
- Mantripragada, R. S. S., C. J. Schreck III, and A. Aiyyer, 2021: Energetics of interactions between African easterly waves and convective coupled Kelvin waves. *Mon. Wea. Rev.*, 149, 3821–3835, https://doi.org/10.1175/MWR-D-21-0003.1.
- Mayta, V. C., G. N. Kiladis, J. Dias, P. L. Silva Dias, and M. Gehne, 2021: Convectively coupled Kelvin waves over

- tropical South America. *J. Climate*, **34**, 6531–6547, https://doi.org/10.1175/JCLI-D-20-0662.1.
- Mekonnen, A., C. D. Thorncroft, A. R. Aiyyer, and G. N. Kiladis, 2008: Convectively coupled Kelvin waves over tropical Africa during the boreal summer: Structure and variability. *J. Climate*, 21, 6649–6667, https://doi.org/10.1175/2008JCLI2008.1.
- Mounier, F., G. N. Kiladis, and S. Janicot, 2007: Analysis of the dominant mode of convectively coupled Kelvin waves in the West African monsoon. *J. Climate*, 20, 1487–1503, https://doi. org/10.1175/JCLI4059.1.
- Nolan, D. S., 2007: What is the trigger for tropical cyclogenesis? *Aust. Meteor. Mag.*, **56**, 241–266.
- Núñez Ocasio, K. M., J. L. Evans, and G. S. Young, 2020: A wave-relative framework analysis of AEW–MCS interactions leading to tropical cyclogenesis. *Mon. Wea. Rev.*, 148, 4657– 4671, https://doi.org/10.1175/MWR-D-20-0152.1.
- —, A. Brammer, J. L. Evans, G. S. Young, and Z. L. Moon, 2021: Favorable monsoon environment over eastern Africa for subsequent tropical cyclogenesis of African easterly waves. J. Atmos. Sci., 78, 2911–2925, https://doi.org/10.1175/ JAS-D-20-0339.1.
- Pedregosa, F., and Coauthors, 2011: Scikit-learn: Machine learning in Python. J. Mach. Learn. Res., 12, 2825–2830.
- Peng, M. S., B. Fu, T. Li, and D. E. Stevens, 2012: Developing versus nondeveloping disturbances for tropical cyclone formation. Part I: North Atlantic. *Mon. Wea. Rev.*, 140, 1047– 1066, https://doi.org/10.1175/2011MWR3617.1.
- Reed, R. J., D. C. Norquist, and E. E. Recker, 1977: The structure and properties of African wave disturbances as observed during Phase III of GATE. *Mon. Wea. Rev.*, 105, 317–333, https://doi.org/10.1175/1520-0493(1977)105<0317:TSAPOA> 2.0.CO:2.
- Ruppert, J. H., Jr., A. A. Wing, X. Tang, and E. L. Duran, 2020: The critical role of cloud-infrared radiation feedback in tropical cyclone development. *Proc. Natl. Acad. Sci. USA*, 117, 27884–27892, https://doi.org/10.1073/pnas.2013584117.
- Russell, J. O., and A. Aiyyer, 2020: The potential vorticity structure and dynamics of African easterly waves. *J. Atmos. Sci.*, **77**, 871–890, https://doi.org/10.1175/JAS-D-19-0019.1.
- —, —, J. D. White, and W. Hannah, 2017: Revisiting the connection between African easterly waves and Atlantic tropical cyclogenesis. *Geophys. Res. Lett.*, 44, 587–595, https://doi.org/10.1002/2016GL071236.
- —, —, and —, 2020: African easterly wave dynamics in convection-permitting simulations: Rotational stratiform instability as a conceptual model. *J. Adv. Model. Earth Syst.*, 12, e2019MS001706, https://doi.org/10.1029/2019MS001706.
- Schenkel, B. A., N. Lin, D. Chavas, M. Oppenheimer, and A. Brammer, 2017: Evaluating outer tropical cyclone size in reanalysis datasets using QuikSCAT data. *J. Climate*, 30, 8745–8762, https://doi.org/10.1175/JCLI-D-17-0122.1.
- Schreck, C. J., III, 2015: Kelvin waves and tropical cyclogenesis: A global survey. Mon. Wea. Rev., 143, 3996–4011, https://doi. org/10.1175/MWR-D-15-0111.1.
- —, 2016: Convectively coupled Kelvin waves and tropical cyclogenesis in a semi-Lagrangian framework. *Mon. Wea. Rev.*, 144, 4131–4139, https://doi.org/10.1175/MWR-D-16-0237.1.
- Scikit-learn, 2022a: Scikit-learn v1.1 user guide: Logistic regression. Accessed 31 November 2022, https://scikit-learn.org/1.1/modules/linear\_model.html#logistic-regression.
- ——, 2022b: Scikit-learn v1.1 user guide: Feature selection. Accessed 31 November 2022, https://scikit-learn.org/1.1/modules/feature selection.html#rfe.

- Straub, K. H., and G. N. Kiladis, 2002: Observations of a convectively coupled Kelvin wave in the eastern Pacific ITCZ. *J. Atmos. Sci.*, **59**, 30–53, https://doi.org/10.1175/1520-0469(2002) 059<0030:OOACCK>2.0.CO;2.
- Takayabu, Y. N., 1994: Large-scale cloud disturbances associated with equatorial waves. Part I: Spectral features of the cloud disturbances. J. Meteor. Soc. Japan, 72, 433–449, https://doi. org/10.2151/jmsj1965.72.3\_433.
- Ventrice, M. J., and C. D. Thorncroft, 2013: The role of convectively coupled atmospheric Kelvin waves on African easterly wave activity. *Mon. Wea. Rev.*, 141, 1910–1924, https://doi.org/10.1175/MWR-D-12-00147.1.
- —, and M. A. Janiga, 2012a: Atlantic tropical cyclogenesis: A three-way interaction between an African easterly wave, diurnally varying convection, and a convectively coupled atmospheric Kelvin wave. *Mon. Wea. Rev.*, **140**, 1108–1124, https://doi.org/10.1175/MWR-D-11-00122.1.
- —, and C. J. Schreck III, 2012b: Impacts of convectively coupled Kelvin waves on environmental conditions for Atlantic tropical cyclogenesis. *Mon. Wea. Rev.*, **140**, 2198–2214, https://doi.org/10.1175/MWR-D-11-00305.1.
- Wang, Z., 2012: Thermodynamic aspects of tropical cyclone formation. J. Atmos. Sci., 69, 2433–2451, https://doi.org/10.1175/JAS-D-11-0298.1.
- —, 2014: Role of cumulus congestus in tropical cyclone formation in a high-resolution numerical model simulation. *J. Atmos. Sci.*, 71, 1681–1700, https://doi.org/10.1175/JAS-D-13-0257.1.
- ——, 2018: What is the key feature of convection leading up to tropical cyclone formation? *J. Atmos. Sci.*, **75**, 1609–1629, https://doi.org/10.1175/JAS-D-17-0131.1.
- —, M. T. Montgomery, and T. J. Dunkerton, 2010: Genesis of pre-Hurricane Felix (2007). Part I: The role of the easterly wave critical layer. J. Atmos. Sci., 67, 1711–1729, https://doi. org/10.1175/2009JAS3420.1.
- Wheeler, M., and G. N. Kiladis, 1999: Convectively coupled equatorial waves: Analysis of clouds and temperature in the wavenumber–frequency domain. *J. Atmos. Sci.*, **56**, 374–399, https://doi.org/10.1175/1520-0469(1999)056<0374:CCEWAO> 2.0.CO:2.
- Wing, A. A., 2022: Acceleration of tropical cyclone development by cloud-radiative feedbacks. *J. Atmos. Sci.*, **79**, 2285–2305, https://doi.org/10.1175/JAS-D-21-0227.1.
- —, and K. A. Emanuel, 2014: Physical mechanisms controlling self-aggregation of convection in idealized numerical modeling

- simulations. J. Adv. Model. Earth Syst., 6, 59–74, https://doi.org/ 10.1002/2013MS000269.
- —, S. J. Camargo, and A. H. Sobel, 2016: Role of radiative–convective feedbacks in spontaneous tropical cyclogenesis in idealized numerical simulations. *J. Atmos. Sci.*, 73, 2633–2642, https://doi.org/10.1175/JAS-D-15-0380.1.
- —, and Coauthors, 2019: Moist static energy budget analysis of tropical cyclone intensification in high-resolution climate models. *J. Climate*, 32, 6071–6095, https://doi.org/10.1175/ JCLI-D-18-0599.1.
- Wu, S.-N., B. J. Soden, and D. S. Nolan, 2021: Examining the role of cloud radiative interactions in tropical cyclone development using satellite measurements and WRF simulations. *Geophys. Res. Lett.*, 48, e2021GL093259, https://doi.org/10. 1029/2021GL093259.
- Yanai, M., S. Esbensen, and J.-H. Chu, 1973: Determination of bulk properties of tropical cloud clusters from large-scale heat and moisture budgets. J. Atmos. Sci., 30, 611–627, https://doi.org/10.1175/1520-0469(1973)030<0611:DOBPOT> 2.0.CO;2.
- Yang, B., and Z.-M. Tan, 2020: Interactive radiation accelerates the intensification of the midlevel vortex for tropical cyclogenesis. J. Atmos. Sci., 77, 4051–4065, https://doi.org/10.1175/ JAS-D-20-0094.1.
- —, J. Nie, and Z.-M. Tan, 2021: Radiation feedback accelerates the formation of Typhoon Haiyan (2013): The critical role of mid-level circulation. *Geophys. Res. Lett.*, 48, e2021GL094168, https://doi.org/10.1029/2021GL094168.
- Yang, G.-Y., B. Hoskins, and J. Slingo, 2007: Convectively coupled equatorial waves. Part II: Propagation characteristics. J. Atmos. Sci., 64, 3424–3437, https://doi.org/10.1175/JAS4018.1.
- Zawislak, J., 2020: Global survey of precipitation properties observed during tropical cyclogenesis and their differences compared to nondeveloping disturbances. *Mon. Wea. Rev.*, 148, 1585–1606, https://doi.org/10.1175/MWR-D-18-0407.1.
- —, and E. J. Zipser, 2014: A multisatellite investigation of the convective properties of developing and nondeveloping tropical disturbances. *Mon. Wea. Rev.*, **142**, 4624–4645, https://doi. org/10.1175/MWR-D-14-00028.1.
- Zhang, B., B. J. Soden, G. A. Vecchi, and W. Yang, 2021: The role of radiative interactions in tropical cyclone development under realistic boundary conditions. *J. Climate*, 34, 2079– 2091, https://doi.org/10.1175/JCLI-D-20-0574.1.